Neutrino mass bounds from leptogenesis with ULYSSES

Bachelor Thesis
submitted to the

University of Münster
Institute for Theoretical Physics

by
Nigel Warning

First Examiner: Jun.-Prof. Dr. Kai Schmitz
Second Examiner: Prof. Dr. Michael Klasen

September 23, 2025

Declaration of Academic Integrity

I hereby confirm that this thesis, entitled *Neutrino mass bounds from leptogenesis with ULYSSES*, is solely my own work and that I have used no sources or aids other than the ones stated. All passages in my thesis for which other sources, including electronic media, have been used, be it direct quotes or content references, have been acknowledged as such and the sources cited. I am aware that plagiarism is considered an act of deception which can result in sanction in accordance with the examination regulations.

I confirm that I am aware that my work may be cross-checked with other texts to identify possible similarities and that it may be stored in a database for this purpose.

I confirm that I have not submitted the following thesis in part or whole as an examination paper before.

(date, signature of student)

Abstract

To explain the measured quantities of baryons in the universe as well as the absence of large scale antimatter structures it is necessary to introduce a new mechanism in the evolution of the early universe which creates a baryon asymmetry. A favoured model for this is leptogenesis. This theory is based on expanding the standard model (SM) with heavy right handed neutrinos (RHNs) which decay in a CP violating fashion, creating a $B-L$ asymmetry which is then transferred into the desired baryon asymmetry using sphaleron processes [1, 2]. Next to the fact that leptogenesis can correctly predict the baryon-to-photon ratio η_B, it is also very well motivated because it uses the same RHNs as driving force as the seesaw model, a theory explaining the light neutrino masses observed in oscillation experiments [3]. Additionally, the neutrino parameters are decisive for the results of the theory, so that, in principle, it can be tested in experiment. The dynamics of leptogenesis is described with a set of semi-classical Boltzmann equations. `ULYSSES` is the first publicly available code that solves these equations numerically and explores the multidimensional parameter space [4, 5]. The goal of this work is to test the applicability of the code by reproducing the analysis conducted in [6] and determining neutrino mass bounds. For the simplest leptogenesis scenario the analysis yields the upper bounds $m_{1,2} < 0.119\,\text{eV}$, $m_3 < 0.129\,\text{eV}$ on the light neutrino mass eigenstates for normal mass ordering (NO), which leads to a bound on the mass scale of $\overline{m} < 0.212\,\text{eV}$. In the case of inverted mass ordering (IO) the bounds read $m_3 < 0.117\,\text{eV}$, $m_{1,2} < 0.127\,\text{eV}$ with $\overline{m} < 0.214\,\text{eV}$. The mass of the decaying heavy neutrino is restricted by the lower bound $M_1 > 2.88 \cdot 10^9\,\text{GeV}$. The results are in agreement with the literature [7] and working with `ULYSSES` turns out to be very straightforward because of the code structure and the already existing applications. This leads to the conclusion that it is a very useful tool and suitable for dealing with leptogenesis.

Contents

1 Introduction

Nowadays, the evolution of our universe is described with a standard model of cosmology starting with the Big Bang, after which an inflationary phase follows until, finally, the expansion is governed by the composition of the energy densities of matter, radiation and dark energy [2, 8]. Their contribution to the full energy density now has been analysed with the cosmic microwave background (CMB) and is expressed with density parameters Ω which relate the energy density to the critical density of a flat spacetime: $\Omega_{\text{dark energy}} = 0.73 \pm 0.04$, $\Omega_{\text{matter}} = 0.27 \pm 0.04$ and $\Omega_B = 0.044 \pm 0.004$ [9]. The parameter Ω_B describes the contribution of baryonic matter so that the difference to Ω_{matter} constitutes of dark matter [2].

Still, a lot of mysteries remain in this model, e.g. regarding the dark matter or dark energy. This work deals with the subject of the baryon energy density or, in different terms, the ratio of the baryon to photon number density η_B. According to CMB data the value reads [10]

$$\eta_B^{\text{CMB}} = (6.12 \pm 0.04) \cdot 10^{-10} \ . \tag{1}$$

Why does this ratio have this specific value? In fact, there is another mystery associated with this question. It can be argued that there are no large scale structures consisting of antimatter within less than cosmic distance scales from us and that therefore our universe is dominated by matter over antimatter [11]. Assuming the baryon and antibaryon number densities to be symmetric would also lead to a problem in the evolution of the early universe. As the universe cools down to temperatures of $\mathcal{O}(1\,\text{GeV})$ the inverse annihilation process of baryons and antibaryons becomes ineffective which causes a significant reduction of the baryon and antibaryon number densities. In this case the baryon-to-photon ratio is expected to be [12]

$$\frac{n_B}{n_\gamma} = \frac{n_{\overline{B}}}{n_\gamma} \approx 10^{-18} \ . \tag{2}$$

This value however violates the data presented in (1). Therefore, at an energy scale of $\mathcal{O}(1\,\text{GeV})$ an asymmetry in the baryon number must have existed. The measured η_B is in fact the ratio of the matter and antimatter number density asymmetry compared to the number density of photons [2]:

$$\eta_B = \frac{n_B - n_{\overline{B}}}{n_\gamma} \ . \tag{3}$$

On the other hand, after an inflationary phase the total baryon number needs to be set to $B = 0$ as an initial condition for the hot early universe [1]. These considerations then lead to the conclusion that there must be some physical mechanism that generated a primordial matter-antimatter asymmetry.

Such mechanisms are referred to as baryogenesis. This work deals with the leptogenesis mechanism as proposed by Fukugita and Yanagida [13], which introduces heavy RHNs as an extension of the SM. With these new particles a $B - L$ asymmetry is generated first and then transferred into a baryon asymmetry.

The text is structured as follows. Section 2 deals with the theoretical background of baryogenesis models and the sphaleron processes, which play a crucial role in leptogenesis. Section 3 is about the neutrino sector in the SM as well as the added RHNs and features a short introduction to the type I seesaw mechanism. In section 4 the Boltzmann equations for the simplest case of leptogenesis are derived and the analytical approximations for the reaction rates are reviewed shortly. Section 5 focuses on the numerical analysis of the Boltzmann equations with the program `ULYSSES`. The structure of the code is presented together with the adjustments conducted here. The analysis yields constraints on the neutrino parameters. Finally, the results and the applicability of `ULYSSES` are discussed in section 6.

2 Theoretical Foundations

2.1 Sakharov conditions

In the seminal work from Sakharov [14] three conditions were formulated which must be fulfilled by any theory of baryogenesis in order for the universe to go from an initial symmetric state into the matter dominated state today. Taken from [1] they read:

1. Baryon-number must be violated, as the hot early universe is considered in an initial state of $B = 0$ and needs to evolve into a final state $B \neq 0$.

2. The process must include C and CP violation. Since the universe is even under charge conjugation at first and becomes odd under charge conjugation once it is matter dominated the relevant process can't be invariant under C or CP conjugation [2]. Additionally, without any CP asymmetry, the reaction rates for the generation and destruction of matter and antimatter would be identical, in which case no baryon asymmetry could be created.

3. If all physical properties and processes were in thermal equilibrium, the system would be stationary. Thus, in order to have a time evolution, a departure from thermal equilibrium is necessary.

Because of these conditions baryogenesis naturally works very well with grand unified theories (GUT) [1]. GUTs extend the gauge group of the SM of particle physics [3]

$$SU(3)_C \times SU(2)_L \times U(1)_Y \tag{4}$$

by adding new gauge symmetries. For this they introduce new heavy particles whose decays can fulfil the Sakharov conditions. The simplest GUT goes to a $SU(5)$, increasing the rank of the SM by 1, which conserves $B-L$. In this GUT only a $B+L$ asymmetry can be generated. However, at the temperature range which is relevant for baryogenesis, sphaleron processes are in thermal equilibrium [15]. These processes also conserve $B-L$ and violate $B+L$, so that any asymmetry is washed out again and B is reduced to its equilibrium value. Instead, it is necessary to go up to a GUT based on $SO(10)$, where RHNs and $B-L$ gauge bosons are included. This way, the $B-L$ symmetry is broken at the GUT scale and the decay of RHNs then creates a $B-L$ asymmetry. Finally, this asymmetry is transferred into a B asymmetry via the above mentioned sphaleron process [1].

2.2 Sphaleron process

The sphaleron process is a non-perturbative theory describing changes in the baryon and lepton number. It is already a part of the SM and arises from the chiral nature of the weak interaction, which causes B and L to not be conserved [16]. Following the notation from [2] the B and L currents are expressed as

$$J^B_\mu = \frac{1}{3}\sum_i (\overline{q_i}\gamma_\mu q_i + \overline{u_i}\gamma_\mu u_i + \overline{d_i}\gamma_\mu d_i) \ , \tag{5}$$

$$J^L_\mu = \sum_i (\overline{l_i}\gamma_\mu l_i + \overline{e_i}\gamma_\mu e_i) \ , \tag{6}$$

where q_i and l_i describe the left handed quark and lepton doublets, while u_i, d_i and e_i represent the two right handed quark and the one right handed lepton singlet respectively. The sum goes over all generations. The divergence of the currents is non vanishing and given by the chiral anomaly [1, 2]

$$\partial^\mu J^B_\mu = \partial^\mu J^L_\mu = \frac{N_f}{32\pi^2}(-g^2 W^I_{\mu\nu}\tilde{W}^{I\mu\nu} + g'^2 B_{\mu\nu}\tilde{B}^{\mu\nu}) \ , \tag{7}$$

with the $SU(2)_L$ gauge field $W_{\mu\nu}$ and the $U(1)_Y$ gauge field $B_{\mu\nu}$ and their respective gauge couplings g and g'. (7) shows that $\partial^\mu J^B_\mu \neq 0$, $\partial^\mu J^L_\mu \neq 0$ and $\partial^\mu (J^B_\mu - J^L_\mu) = 0$. Therefore, in the SM, $B-L$ is conserved while $B+L$ is violated. At this point, the contribution of the $U(1)_Y$ hypercharge gauge field can be neglected as it does not contribute to the later discussed transitions between vacuum states [1]. The change in B or L from an initial time t_i up to a final time t_f can be expressed as

$$B(t_f) - B(t_i) = \int_{t_i}^{t_f} dt \int d^3x \partial^\mu J^B_\mu = N_f(N_{CS}(t_f) - N_{CS}(f_i) \ , \tag{8}$$

where N_{CS} are the Chern-Simons numbers [2]

$$N_{CS} = \frac{g^3}{96\pi^2}\int d^3x \epsilon_{ijk}\epsilon^{IJK} W^{Ii} W^{Jj} W^{Kk} \ . \tag{9}$$

In a vacuum state the Higgs field reaches the minimum of its potential A_μ. Choosing the gauge $A_0^a = 0$, W^{Ii} are pure gauge configurations and N_{CS} are the gauge field winding numbers and, with that, integers [1]. A change in the Chern-Simons number ΔN_{CS} then corresponds to a change in the number of baryons or leptons by $\Delta B = \Delta L = N_f \Delta N_{CS}$, where in the SM the number of generations $N_f = 3$ [16]. In a non-abelian gauge theory there exist infinitely many degenerate ground states [2] which translates to an infinite amount of vacuum states where the Higgs field reaches the same minimum value with different Chern-Simons numbers. The minimum static energy of the gauge Higgs field can then be expressed as a function of N_{CS} with minima at full integer values of N_{CS} [7]. Static solutions of the equation of motion give a maximum at half integer values of N_{CS}. These make up an energy barrier with the height E_{sph}, the sphaleron energy, which needs to be crossed for a vacuum transition [17].

One possibility to traverse the barrier is via tunnelling. These transitions are called instantons [8]. However the tunnelling rate determined from the instanton action is of the order of $\mathcal{O}(10^{-165})$ and therefore these processes are negligible [16].

The situation changes significantly when considering the hot early universe as a thermal bath. With a temperature greater than E_{sph} thermal fluctuations allow transitions over the energy barrier [15], which are referred to as electroweak sphalerons [8]. The $(B+L)$-violating sphaleron processes can be in thermal equilibrium in the early expanding universe at which point the processes play a significant role and reduce B to its equilibrium number B^{eq}, which can be unequal to zero if there already exists an asymmetry in the number of leptons, as $B-L$ is still conserved [1]. The temperature range in which the sphaleron processes are in thermal equilibrium is determined to be approximately [2]

$$T_{EW} \sim 100\,\text{GeV} < T < T_{sph} \sim 10^{12}\ \text{GeV}\ . \tag{10}$$

2.3 Transfer from $B-L$ to B asymmetry

In the theory of leptogenesis the above described sphaleron processes play a crucial role as they enable to go from a $B-L$ asymmetry to the desired baryon asymmetry. In order to quantify this transition, all interactions which are in thermal equilibrium in the temperature range of (10) are compared via the chemical potentials of the participating particles. Each doublet and singlet as well as the Higgs boson is assigned a chemical potential, leading to $5N_f + 1$ variables. Following the notation from (5) and (6) the chemical potentials are labelled as μ_{qi}, μ_{ui} and μ_{di} for the quarks, μ_{li} and μ_{ei} for the leptons and μ_ϕ for the Higgs. The chemical potentials are constrained by the processes in thermal equilibrium [18]. Four processes are of interest: First the $SU(2)$ electroweak N_{CS}-changing transition, which

affects only left handed particles [1]

$$\sum_i (3\mu_{qi} + \mu_{li}) = 0 \ . \tag{11}$$

The sum goes over all generations and the equation states that B and L change by the same amount, for $B-L$ is conserved in the sphaleron process. Next there are $SU(3)$ QCD sphaleron procecesses [19], which relate the left and the right handed quarks with [1]

$$\sum_i (2\mu_{qi} - \mu_{ui} - \mu_{di}) = 0 \ . \tag{12}$$

This equation ensures that the chiral quark number changes by the same amount for each quark flavour. Furthermore, there are the Yukawa interactions, which describe the connection between the left handed doublets, the right handed singlets and the Higgs boson [1]

$$-\mu_{qi} + \mu_{dj} = \mu_{qi} - \mu_{uj} = -\mu_{li} + \mu_{ej} = \mu_\phi \ . \tag{13}$$

The temperature region in which the Yukawa interactions are in thermal equilibrium is more restricted than the ones of the other processes. Because of this there exist separate temperature regions in which different charges are conserved. These effects are neglected in this work however as they are expected to only have a small influence on the simplest leptogenesis model [2].

The chemical potentials are related to the asymmetry between particle and antiparticle number density via the appropriate partition function [1]

$$Z(T, V, \mu) = \mathrm{Tr}\, e^{\beta\left(\sum_i \mu_i Q_i - H\right)} \ , \tag{14}$$

with the charge operator Q_i for the corresponding quarks, leptons and the Higgs as well as the Hamiltonian H. The asymmetry is then given as [1]

$$n_i - n_{\bar{i}} = -\frac{\partial}{\partial \mu_i} \frac{T}{V} \ln Z(T, V, \mu) = \frac{g_i T^2}{6} \mu_i + O((\beta\mu_i)^3) \tag{15}$$

for fermions in a non-interacting gas of massless particles. Here g_i denotes the number of internal degrees of freedom and, assuming small chemical potentials in comparison to the relevant temperature region $\beta\mu_i \ll 1$, only the leading μ_i term is considered. With this the last condition, the vanishing of the total hypercharge, is given by [1]

$$\sum_i (\mu_{qi} + 2\mu_{ui} - \mu_{di} - \mu_{li} - \mu_{ei}) = 2\mu_\phi \ . \tag{16}$$

Using (15) it is possible to formulate an explicit expression for the baryon and lepton number densities [1]

$$n_B = \frac{T^2}{6} \sum_i (2\mu_{qi} + \mu_{ui} + \mu_{di}) \ , \tag{17}$$

$$n_{L_i} = \frac{T^2}{6}(2\mu_{li} + \mu_{ei}) \ . \tag{18}$$

The quark chemical potentials are family independent and, as another simplification, it will be assumed that the lepton chemical potentials are family independent as well. Then (11), (12) and (13) in addition to (16) make up a set of coupled equations that can be solved for one arbitrary chemical potential. Solving the equations for μ_l gives [1]

$$n_B = -\frac{T^2}{6}\frac{4N_f}{3}\mu_l \ , \tag{19}$$

$$n_L = \frac{T^2}{6}\frac{14N_f^2 + 9N_f}{6N_f + 3}\mu_l \ . \tag{20}$$

Combining (19) and (20) yields an expression connecting B with $B - L$ [1]

$$B = c_S(B - L) \ , \tag{21}$$

$$L = (c_S - 1)(B - L) \ , \tag{22}$$

$$c_S = \frac{8N_f + 4}{22N_f + 13} = \frac{28}{79} \ , \tag{23}$$

where the value for the coefficient c_S is determined for $N_f = 3$. For more details on the left out calculations see appendix A. In general, the ratio c_S also depends on the temperature when it reaches the electroweak transition [20]. For the purpose of this work c_S is treated as a constant and then (21) shows that, since $B - L$ remains constant after the leptogenesis process, the sphaleron processes are accounted for with this factor. Therefore, the Baryon number measured today $B(t_0)$ is determined by the value of $B - L$ at the time t_f at which leptogenesis has stopped [1]

$$B(t_0) = c_S(B - L)(t_f) \ . \tag{24}$$

3 Neutrino parameters

3.1 Neutrinos in and beyond the SM

According to the gauge group of the SM as presented in (4), quarks and leptons are organised in doublets with left handed chirality and singlets with right handed chirality. The neutrinos are part of the lepton sector, consisting of [3]

$$\begin{aligned} \begin{pmatrix} \nu_{eL} \\ e_L \end{pmatrix} \quad &, \quad e_R \ , \\ \begin{pmatrix} \nu_{\mu L} \\ \mu_L \end{pmatrix} \quad &, \quad \mu_R \ , \\ \begin{pmatrix} \nu_{\tau L} \\ \tau_L \end{pmatrix} \quad &, \quad \tau_R \ , \end{aligned} \tag{25}$$

where e, μ, τ are the charged leptons and the neutrinos are denoted in the charged lepton mass basis states $\nu_{e,\mu,\tau}$. The different neutrino flavours are defined via the coupling with the corresponding charged lepton during the weak interaction, e.g. with the W^+ gauge boson [21]

$$W^+ \to e^+ \nu_e \ . \tag{26}$$

The neutrinos are also characterised by their lepton number of $L = \pm 1$, with the negative value for antineutrinos, their hypercharge Y and the absence of any colour or electric charge. Therefore, they can only interact via the weak interaction. A very important aspect of the neutrino sector in the SM is that only left handed neutrinos exist. Then, it is not possible to construct a Dirac mass term. Since also, there are only Higgs doublets and the SM Lagrangian is renormalisable, neutrinos are massless in the SM [3] and, in fact, no non-zero neutrino mass was found in a direct measurement [21].

However flavour oscillations, predicted by Bruno Pontecorvo [22], have been discovered in experiment [23, 24]. This effect requires neutrino masses and new physics beyond the SM [8]. As mentioned above neutrinos can be described in the charged lepton mass basis states ν_α, denoted with Greek subscripts $\alpha = e, \mu, \tau$, or in terms of their mass eigenstate basis ν_i, denoted with Roman subscripts $i = 1, 2, 3$, where each neutrino mass eigenstate ν_i is identified with a definite mass m_i. The two bases are misaligned by the Pontecorvo-Maki-Nakagawa-Sakata (PMNS) matrix U_{PMNS} [3, 8]

$$|\nu_\alpha\rangle = \sum_i U^*_{\alpha i} \, |\nu_i\rangle \ . \tag{27}$$

In the standard PDG convention [25] U_{PMNS} is considered to be unitary with orthogonal flavour and mass eigenstates and is described with three mixing angles, one CP violating phase and two Majorana phases

$$U = \begin{pmatrix} 1 & 0 & 0 \\ 0 & c_{23} & s_{23} \\ 0 & -s_{23} & c_{23} \end{pmatrix} \begin{pmatrix} c_{13} & 0 & s_{13} e^{-i\delta} \\ 0 & 1 & 0 \\ -s_{13} e^{i\delta} & 0 & c_{13} \end{pmatrix} \begin{pmatrix} c_{12} & s_{12} & 0 \\ -s_{12} & c_{12} & 0 \\ 0 & 0 & 1 \end{pmatrix} P \ , \tag{28}$$

where $s_{ab} = \sin\theta_{ab}$, $c_{ab} = \cos\theta_{ab}$ with the mixing angles θ_{ab} and the CP violating phase δ. The matrix P contains the Majorana phases α_{21} and α_{31}

$$P = \text{diag}(1, e^{i\alpha_{21}/2}, e^{i\alpha_{31}/2}) \ . \tag{29}$$

The Majorana phases $\alpha_{1,2}$ don't affect neutrino oscillation but instead neutrinoless double β-decay [21]. This is also the parameterisation used in the `ULYSSES` code, as explained in section 5.1. In general, new physics operators at energy scales beyond the SM can lead to nonunitary U_{PMNS}. One example is the inclusion of three RHNs which creates a small deviation from the unitary matrix, as discussed in section 3.2. While the flavour eigenstates

are no longer orthogonal, the theory of flavour oscillation remains unitary in time evolution [3, 26].

The charged lepton mass basis states are associated with a specific flavour but not with a well defined mass. A definite flavour state can be expressed as a superposition of mass eigenstates, like in (27), each with a well defined mass. Because of the different masses the relative phases of the mass eigenstates change over time. The time evolution of a plane wave solution of the Schrödinger equation for the neutrino mass eigenstates reads [8]

$$|\nu_i(x,t)\rangle = e^{-iE_i t} e^{ipx} |\nu_i\rangle \approx e^{-i\frac{m_i^2}{2E}L} |\nu_i\rangle \tag{30}$$

after a traversed distance of $x = L$ and assuming the neutrino to be relativistic. Then, the probability for going from one initial flavour state $|\nu_\alpha\rangle$ to a final state $|\nu_\beta\rangle$ is [8]

$$\begin{aligned} P(\nu_\alpha \to \nu_\beta) = \delta_{\alpha\beta} &- 4\sum_{i>j} \mathrm{Re}(U^*_{\alpha i} U_{\beta i} U_{\alpha j} U^*_{\beta j}) \sin^2\left(\frac{(m_i^2 - m_j^2)L}{4E}\right) \\ &+ 2\sum_{i>j} \mathrm{Im}(U^*_{\alpha i} U_{\beta i} U_{\alpha j} U^*_{\beta j}) \sin^2\left(\frac{(m_i^2 - m_j^2)L}{2E}\right) . \end{aligned} \tag{31}$$

This is a simplified picture, only taking into account plane wave solutions and describing oscillations in the vacuum. In principle, one would have to consider more aspects to the problem, e.g. describing the neutrino states as wave packets to enable a localisation, thus introducing a coherence length. Yet, this very simple approach suffices to show, that the mass squared differences $m_i^2 - m_j^2$ of two neutrinos can be read off the oscillation length, while the amplitude of the oscillation yields information about the mixing angles [8, 21].

The angles and CP violating phase according to neutrino oscillation data [27, 28, 29] are measured as

$$\theta_{12} = 31^\circ - 36^\circ , \quad \theta_{23} = 40^\circ - 52^\circ , \quad \theta_{13} = 8.2^\circ - 8.9^\circ , \tag{32}$$

$$\delta = 0^\circ - 45^\circ \quad \& \quad 110^\circ - 360^\circ . \tag{33}$$

Since it is not possible to measure the mass of one neutrino mass eigenstate directly, the definite mass scale remains unknown. The experimental results show a hierarchical order of the neutrino masses with a small and a large mass difference. The small mass splitting is observed from solar neutrino experiments. Using the best fit to the PDG NuFIT 5.1 data [27] the mass splitting reads

$$\Delta m^2_{\mathrm{sol}} = m_2^2 - m_1^2 = 7.42 \cdot 10^{-5} \mathrm{eV}^2 . \tag{34}$$

Atmospheric neutrinos give values for the large mass splitting, however the measurements still leave a sign ambiguity. This leads to the two different

scenarios normal ordering (NO), with $m_1 < m_2 \ll m_3$ and

$$(\Delta m^{\mathrm{NO}}_{\mathrm{atm}})^2 = m_3^2 - m_1^2 \simeq 2.515 \cdot 10^{-3}\,\mathrm{eV}^2 \ , \tag{35}$$

and inverse ordering (IO), with $m_3 \ll m_1 < m_2$ and [27]

$$(\Delta m^{\mathrm{IO}}_{\mathrm{atm}})^2 = m_2^2 - m_3^2 \simeq 2.498 \cdot 10^{-3}\,\mathrm{eV}^2 \ . \tag{36}$$

Keeping the two orderings in mind, the experimental results Δm_{sol} and Δm_{atm} allow to express all neutrino masses with just one unknown mass parameter, conveniently chosen to be the lightest neutrino mass m, which refers to m_1 for NO and m_3 for IO.

3.2 RHNs and the seesaw model

In the SM, particles like the charged leptons gain their masses from Dirac mass terms, which describe an interaction between a left- and a right handed particle. The Dirac mass terms arise from the gauge invariant interaction between the electroweak doublets l_α, singlets α_R and the Higgs doublet ϕ, which are connected with Yukawa coupling constants [8]. As an example, using the left handed electron and neutrino doublet l_e and the right handed electron e_R from (25)

$$l_e = \begin{pmatrix} \nu_{eL} \\ e_L \end{pmatrix} \quad , \quad e_R \ ,$$

the electron mass is constructed from the interaction term with the coupling constant Y_e [3]

$$Y_e \overline{l_e} \phi e_R + h.c. \ . \tag{37}$$

When the Higgs reaches its vacuum expectation value $v = 174\,\mathrm{GeV}$ [4], the electroweak symmetry is broken down to electromagnetism [3]

$$SU(2)_L \times U(1)_Y \to U(1)_Q \ , \tag{38}$$

and from (37) follows the mass term for the electron [1, 3]

$$Y_e v(\overline{e}_L e_R + \overline{e}_R e_L) = Y_e v \overline{e} e \ , \tag{39}$$

with the four component Dirac spinor [3]

$$e = \begin{pmatrix} e_L \\ e_R \end{pmatrix} \ . \tag{40}$$

The electron mass is then given by $m_e = Y_e v$ [1]. Including all three charged leptons, interaction terms between all lepton doublets and singlets are possible and the couplings $Y_{\alpha\beta}$ are collected in a Yukawa matrix. This matrix is diagonalized by choosing the charged lepton mass eigenstate basis, which only leaves three mass terms, one for each charged lepton flavour [3].

Since there are only left handed neutrinos, neutrino Dirac masses cannot be formulated [3, 8]. One possibility of explaining the neutrino masses is the seesaw model, which is based on RHNs. Extending the SM with a $B-L$ gauge symmetry, e.g. a $U(1)_{B-L}$ group, requires three RHNs [2]. They are denoted as ν_R and are electroweak singlets with zero electric charge and hypercharge [3]. They don't participate in the weak interaction and are therefore referred to as *sterile* neutrinos [8]. The RHNs can be expressed in terms of a four component spinor

$$N = \begin{pmatrix} \nu_R^c \\ \nu_R \end{pmatrix} \tag{41}$$

that includes ν_R and its CP conjugate field $\nu_R^c = i\sigma_2 \nu_R^*$, which behaves like a left handed antineutrino field [3]. In contrary to the Dirac spinor in (40), the so called Majorana spinor in (41) has only two degrees of freedom and is its own CP conjugate $N^c = N$. Because of this, the Majorana particle is referred to as being its own antiparticle. At energies below the $B-L$ symmetry breaking scale the RHNs acquire their mass and the effective Lagrangian for the lepton mass sector then reads [3]

$$\mathcal{L}_{\text{mass}}^{\text{lepton}} = -\phi \bar{l}_i Y_{ij}^e e_{Rj} - \tilde{\phi} \bar{l}_i Y_{ia}^\nu \nu_{Ra} - \frac{1}{2} \overline{\nu_{Ra}^c} M_R^{ab} \nu_{Rb} + h.c. \ , \tag{42}$$

with $\tilde{\phi} = i\sigma_2 \phi^*$, the Higgs doublet with opposite hypercharge $-1/2$. In this notation, $i, j = 1, 2, 3$ label the SM particles and $a, b = 1, 2, 3$ denote the RHNs in an arbitrary basis. The first term generates the charged lepton masses as discussed above. The second term connects left and right handed neutrinos and, after electroweak symmetry breaking, yields a neutrino Dirac mass term [3]

$$\tilde{\phi} \bar{l}_i Y_{ia}^\nu \nu_{Ra} \to Y_{ia}^\nu v \overline{\nu}_{Li} \nu_{Ra} \ , \tag{43}$$

the Yukawa couplings Y_{ia}^ν are organised in the Yukawa matrix Y. Together with v it makes up the neutrino Dirac mass matrix [4]

$$m_D = Yv \ . \tag{44}$$

The third term is the Majorana mass term of the RHNs. The factor of $1/2$ accounts for the difference in the degrees of freedom between a Majorana and a Dirac particle and the associated masses M_R^{ab} in the Majorana mass matrix M_R are not attached to the scale of the SM but rather to a higher energy scale like unification. The left handed neutrinos don't combine to Majorana mass terms as it is forbidden by electroweak gauge invariance due to their hypercharge. The mass terms in the effective Lagrangian can be summarised neatly in a matrix form [3]

$$\begin{pmatrix} \overline{\nu_L} & \overline{\nu_R^c} \end{pmatrix} \begin{pmatrix} 0 & m_D \\ m_D^T & M_R \end{pmatrix} \begin{pmatrix} \nu_L^c \\ \nu_R \end{pmatrix} \ , \tag{45}$$

where m_D and M_R are 3×3 matrices and ν_L and ν_R contain the left and right handed neutrinos of all three generations. The matrix is diagonalized using a rotation matrix U with the angle matrix θ [3]

$$U \begin{pmatrix} 0 & m_D \\ m_D^T & M_R \end{pmatrix} U^T = \begin{pmatrix} m_- & 0 \\ 0 & m_+ \end{pmatrix} . \tag{46}$$

ν and N are the corresponding light and heavy neutrino mass eigenstates to the eigenvalues m_- and m_+. Since the Majorana masses are not tied to the SM energy scale and therefore expected to be very heavy while m_D is of the order of the electroweak scale [2], $M_R \gg m_D$. Then $\theta \simeq m_D M_R^{-1}$ and with that [3]

$$U \approx \begin{pmatrix} 1 - \frac{1}{2}\theta\theta^\dagger & \theta \\ \theta^\dagger & 1 - \frac{1}{2}\theta\theta^\dagger \end{pmatrix} , \tag{47}$$

$$N \approx \nu_R + \theta\nu_L^c \quad , \quad \nu \approx \nu_l - \theta\nu_R^c . \tag{48}$$

The heavy neutrino eigenstates mainly constitute of the RHNs with a small admixture of the SM left handed ones, for the light neutrino eigenstates the opposite applies. The large eigenmass can be approximated with $m_+ \approx M_R$. The light neutrino eigenmass $m_- = m^\nu$, also referred to as effective left handed neutrino Majorana mass, is given by the seesaw formula

$$m^\nu \approx -m_D M_R^{-1} m_D^T , \tag{49}$$

where the minus sign is typically ignored as it can be absorbed into the fermion field [3]. The seesaw formula (49) emphasises the advantage of this model. Not only do the neutrino masses arise from the same process of spontaneous symmetry breaking like the other particles in the SM, at the same time the model also gives a natural explanation for their peculiar smallness through the heavy Majorana masses M_R. The light neutrino mass matrix m^ν is diagonalized with a unitary matrix V_ν

$$V_\nu m^\nu V_\nu^T = \mathrm{diag}(m_1, m_2, m_3) = \hat{m} . \tag{50}$$

Then, in the flavour basis, where the charged lepton mass matrix and the RHN mass matrix M_R are chosen diagonal, U_{PMNS} can be defined with (47) and (50)

$$\begin{pmatrix} \nu_e \\ \nu_\mu \\ \nu_\tau \end{pmatrix} = \left(1 - \frac{1}{2}\theta\theta^\dagger\right) V_\nu^\dagger \begin{pmatrix} \nu_1 \\ \nu_2 \\ \nu_3 \end{pmatrix} = U_{\mathrm{PMNS}} \begin{pmatrix} \nu_1 \\ \nu_2 \\ \nu_3 \end{pmatrix} . \tag{51}$$

Therefore, in the case of three RHNs, U_{PMNS} is no longer exactly unitary [3]. Nevertheless, since the angle matrix $\theta \approx m_D M_R^{-1}$ is small, m^ν is approximately diagonalized using U_{PMNS}

$$m^\nu \approx U_{\mathrm{PMNS}} \hat{m} U_{\mathrm{PMNS}}^T . \tag{52}$$

The seesaw model introduces many new parameters, e.g. the 3×3 complex entries of m_D. To reduce the number of free parameters, m_D is typically parameterised in a bottom up approach in the flavour basis. Using both (49) and (52) and dropping the minus sign gives the expression [3]

$$m_D \hat{M}^{-1} m_D^T = U_{\text{PMNS}} \hat{m} U_{\text{PMNS}}^T \ , \tag{53}$$

with the diagonalized Majorana mass matrix $\hat{M}$. The equation can be solved for m_D introducing a new orthogonal matrix R, leading to the Casas-Ibarra parameterisation [30]

$$m_D = U_{\text{PMNS}} \sqrt{\hat{m}} R^T \sqrt{\hat{M}} \ . \tag{54}$$

The matrix R itself is described through 6 parameters in the form of 3 complex angles $\omega_j = x_j + i y_j$ [4]

$$R = \begin{pmatrix} 1 & 0 & 0 \\ 0 & c_{\omega_1} & s_{\omega_1} \\ 0 & -s_{\omega_1} & c_{\omega_1} \end{pmatrix} \begin{pmatrix} c_{\omega_2} & 0 & s_{\omega_2} \\ 0 & 1 & 0 \\ -s_{\omega_2} & 0 & c_{\omega_2} \end{pmatrix} \begin{pmatrix} c_{\omega_3} & s_{\omega_3} & 0 \\ -s_{\omega_3} & c_{\omega_3} & 0 \\ 0 & 0 & 1 \end{pmatrix} \ . \tag{55}$$

This way, the 18 parameters of m_D have been expressed using just 6 new parameters together with 12 old ones, which were already a part of the theory. This is a simple picture of the type-I seesaw model, which is all that is necessary for the simplest version of leptogenesis.

4 Thermal leptogenesis

4.1 CP-asymmetry

Leptogenesis is a process close to thermal equilibrium, triggered by the decay of RHNs [1]. The time evolution of the RHN number density n_{N_i} and the number density of the $B-L$ asymmetry n_{B-L} is therefore determined with a set of Boltzmann equations. These equations describe and compare the effects of decays, inverse decays and scatterings with reaction rates and also consider the expansion of the universe. To find a simplified form of the Boltzmann equations, it is useful to derive an expression for the CP-asymmetry ε first. Additionally, ε is an interesting value since CP-asymmetry is a necessary characteristic for a theory of leptogenesis according to the Sakharov conditions (see section 2.1).

The asymmetry ε is defined as [1, 31]

$$\varepsilon_i = \frac{\Gamma_{N_i l} - \Gamma_{N_i \bar{l}}}{\Gamma_{N_i l} + \Gamma_{N_i \bar{l}}} \ , \tag{56}$$

where $\Gamma_{N_i l} = \sum_j \Gamma(N_i \to l_j \phi)$ and $\Gamma_{N_i \bar{l}} = \sum_j \Gamma(N_i \to \bar{l}_j \phi^\dagger)$ are the reaction rates for the decay of the i-th RHN into leptons and the Higgs particle and

the CP inversed case respectively. Lepton flavour interactions are neglected by summing over all lepton flavours, which is known as the *one flavour approximation* [1]. ε_i is derived by considering the Lagrangian and the appropriate Feynman diagrams. The Lagrangian is given by [31]

$$\mathcal{L} = -Y_{ji}\epsilon_{\alpha\beta}\overline{N_i}P_L l_j^\alpha \phi^\beta + h.c. \ , \tag{57}$$

with the left handed lepton doublet $l_j^T = (\nu_j \, l_j^-)$, the Higgs doublet $\phi^T = (\phi^+ \, \phi^0)$ and the Yukawa coupling Y_{ji}. Permutations of α and β are accounted for by $\epsilon_{\alpha\beta} = -\epsilon_{\beta\alpha}$, $\epsilon_{1,2} = 1$. At tree level the decay rates read [31]

$$\Gamma_{N_i l} = \Gamma_{N_i \bar{l}} = \frac{(Y^\dagger Y)_{ii}}{16\pi} M_i \ , \tag{58}$$

and therefore $\varepsilon_i = 0$. A non vanishing CP asymmetry is obtained at one-loop order by calculating the interference terms between the tree level and the one-loop diagrams depicted in (59) for $\Gamma_{N_i l}$. The calculations are displayed in more detail in appendix B.

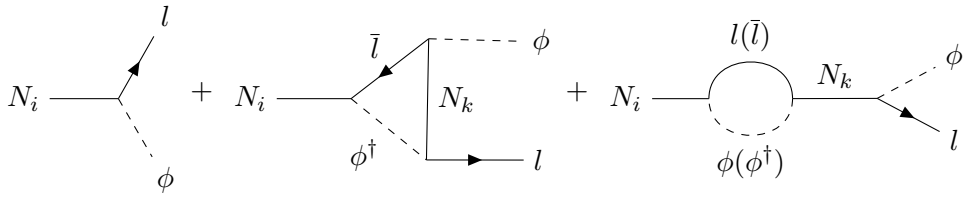

(59)

The correction from the vertex and the wave function respectively read [31]

$$\varepsilon_i(vertex) = \frac{1}{8\pi} \sum_k f(y_k) \frac{\mathrm{Im}\left[(Y^\dagger Y)^2_{ki}\right]}{(Y^\dagger Y)_{ii}} \ , \tag{60}$$

with $y_k = M_k^2/M_i^2$ and the function

$$f(x) = \sqrt{x}\left[1 - (1+x)\ln\left(\frac{1+x}{x}\right)\right] \ ,$$

and

$$\varepsilon_i(wave) = -\frac{1}{8\pi} \sum_{k\neq i} \frac{M_i M_k}{M_k^2 - M_i^2} \frac{\mathrm{Im}\left[(Y^\dagger Y)^2_{ki}\right]}{(Y^\dagger Y)_{ii}} \ . \tag{61}$$

Here, the case of hierarchical heavy neutrinos is studied and, additionally, it is assumed that the lightest RHN, denoted as N_1, dominates leptogenesis. Then only one RHN decay is considered. The sum in (60) can be written as sum over $k \neq i$, since $\mathrm{Im}[(Y^\dagger Y)^2_{ii}] = 0$ [31]. Furthermore, the mass terms in (60) and (61) are approximated as

$$f(y_k) \approx -\frac{M_i}{2M_k} \ ,$$

$$\frac{M_i M_k}{M_k^2 - M_i^2} \approx \frac{M_i}{M_k} \ . \tag{62}$$

With this, the total asymmetry to first loop order reads

$$\varepsilon_1 = \varepsilon_1(vertex) + \varepsilon_1(wave) \approx -\frac{3}{16\pi} \sum_{k \neq 1} \frac{M_1}{M_k} \frac{\mathrm{Im}\left[(Y^\dagger Y)^2_{k1}\right]}{(Y^\dagger Y)_{11}} \ . \tag{63}$$

Different scenarios require other formulas, e.g. when considering small mass differences, where a resonance regime comes into play when the mass differences are of the order of the decay width [32, 33]. Using the neutrino Dirac mass $m_D = Yv$ and the light neutrino mass $m_\nu = -m_D M^{-1} (m_D)^T$ from the seesaw mechanism gives a simplified term [1]

$$\varepsilon_1 = -\frac{3}{16\pi} \frac{M_1}{v^2} \, \mathrm{Im}\, (Y^\dagger m_\nu Y^*)_{11} \ . \tag{64}$$

4.2 Kinetic equations

Having dealt with the CP asymmetry, one can now focus on the Boltzmann equations. For simplicity the subscript 1 is dropped at this point for the RHN N_1 and the asymmetry ε_1. Starting with n_N and taking into account only the decay and inverse decay as well as the expansion of the universe gives [1]

$$\begin{aligned} \dot{n}_N + 3Hn_N = &- \left[\gamma(N \to l\phi) + \gamma(N \to \bar{l}\phi^\dagger)\right] \\ &+ \gamma^{eq}(l\phi \to N) + \gamma^{eq}(\bar{l}\phi^\dagger \to N) \ , \end{aligned} \tag{65}$$

with the Hubble parameter H. The reaction densities γ describe the number of reactions per time and volume and, for a general process $1 + 2 + \cdots \to a + b + \ldots$, they are defined as

$$\gamma(1{+}2{+}\cdots \to a{+}b{+}\ldots) = \int d\Phi f_1(p_1) f_2(p_2) \ldots |\mathcal{M}(1{+}2{+}\cdots \to a{+}b{+}\ldots)|^2 \tag{66}$$

with the phase-space volume element

$$d\Phi = \frac{d^3 p_1}{(2\pi)^3 2E_1} \ldots (2\pi)^4 \delta^4(p_1 + \cdots - p_a - \ldots) \tag{67}$$

and the zero-temperature S-matrix element $\mathcal{M}$ to first approximation [1]. $\Delta L = 2$ processes include virtual intermediate RHNs as propagators and thus don't change n_N, $\Delta L = 1$ scatterings however must be included. One has to consider the s-channel

$$\gamma_{\Delta L=1,s} = \gamma^{eq}(Nl \leftrightarrow \bar{t}q) = \gamma^{eq}(N\bar{l} \leftrightarrow t\bar{q}) \ , \tag{68}$$

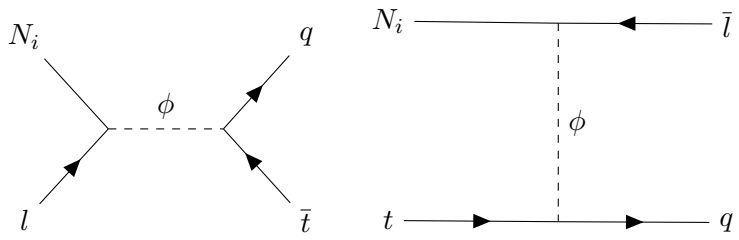

Figure 1: The $\Delta L = 1$ scattering processes [1].

as well as the t-channel [7, 34]

$$\gamma_{\Delta L=1,t} = \gamma^{eq}(Nt \leftrightarrow \bar{l}q) = \gamma^{eq}(N\bar{t} \leftrightarrow l\bar{q}) = \gamma^{eq}(Nq \leftrightarrow \bar{l}t) = \gamma^{eq}(N\bar{q} \leftrightarrow l\bar{t}) \ . \tag{69}$$

The corresponding Feynman diagrams are shown in fig. 1. With this (65) is modified to

$$\begin{aligned}\dot{n}_N + 3Hn_N = &- \left[\gamma(N \to l\phi) + \gamma(N \to \bar{l}\phi^\dagger)\right] + \gamma^{eq}(l\phi \to N) + \gamma^{eq}(\bar{l}\phi^\dagger \to N) \\ &- \left[\gamma(Nl \to \bar{t}q) + \gamma(N\bar{l} \to t\bar{q}) + \gamma(Nt \to \bar{l}q) + \gamma(N\bar{t} \to l\bar{q})\right. \\ &\left. + \gamma(Nq \to \bar{l}t) + \gamma(N\bar{q} \to l\bar{t})\right] + \gamma(\bar{t}q \to Nl) + \gamma(t\bar{q} \to N\bar{l}) \\ &+ \gamma(\bar{l}q \to Nt) + \gamma(l\bar{q} \to N\bar{t}) + \gamma(\bar{l}t \to Nq) + \gamma(l\bar{t} \to N\bar{q}) \ .\end{aligned} \tag{70}$$

In this simple case of leptogenesis one can assume the RHNs to be in kinetic equilibrium and also approximate the phase space distribution functions with the Maxwell-Boltzmann distribution [1], which leads to f being approximated with the equilibrium distribution and a normalisation factor

$$f_1(p) = \frac{n_1}{n_1^{eq}} f^{eq}(p) \ , \tag{71}$$

and therefore

$$\begin{aligned}\gamma(N \to l\phi) &= \frac{n_N}{n_N^{eq}} \gamma^{eq}(N \to l\phi) \ , \\ \gamma(N \to \bar{l}\phi^\dagger) &= \frac{n_N}{n_N^{eq}} \gamma^{eq}(N \to \bar{l}\phi^\dagger) \ .\end{aligned} \tag{72}$$

The same goes for the $\Delta L = 1$ terms, which are summarised as

$$\begin{aligned}\gamma_{\Delta L=1} =&\gamma^{eq}(Nl \to \bar{t}q) + \gamma^{eq}(N\bar{l} \to t\bar{q}) + \gamma^{eq}(Nt \to \bar{l}q) + \gamma^{eq}(N\bar{t} \to l\bar{q}) \\ &+ \gamma^{eq}(Nq \to \bar{l}t) + \gamma^{eq}(N\bar{q} \to l\bar{t}) \\ =&\gamma^{eq}(\bar{t}q \to Nl) + \gamma^{eq}(t\bar{q} \to N\bar{l}) + \gamma^{eq}(\bar{l}q \to Nt) + \gamma^{eq}(l\bar{q} \to N\bar{t}) \\ &+ \gamma^{eq}(\bar{l}t \to Nq) + \gamma^{eq}(l\bar{t} \to N\bar{q}) \\ =&2\gamma_{\Delta L=1,s} + 4\gamma_{\Delta L=1,t} \ .\end{aligned} \tag{73}$$

The decay and inverse decay rate densities are related to the CP asymmetry ε and the total decay width γ_N [1]

$$\gamma^{eq}(N \to l\phi) = \frac{1+\varepsilon}{2}\gamma_N \ ,$$
$$\gamma^{eq}(N \to \bar{l}\phi^\dagger) = \frac{1-\varepsilon}{2}\gamma_N \ , \tag{74}$$

while the remaining reaction rates are rewritten using the CPT invariance [1]

$$\gamma^{eq}(l\phi \to N) = \gamma^{eq}(N \to \bar{l}\phi^\dagger) \ ,$$
$$\gamma^{eq}(\bar{l}\phi^\dagger \to N) = \gamma^{eq}(N \to l\phi) \ . \tag{75}$$

Inserting (72), (73), (74), and (75) into (70) yields

$$\dot{n}_N + 3Hn_N = -\left(\frac{n_N}{n_N^{eq}} - 1\right)(\gamma_N + \gamma_{\Delta L=1}) \ . \tag{76}$$

The equation for n_{B-L} is constructed from the Boltzmann equations for n_B and n_L using [1]

$$n_l = n_l^{eq} - \frac{1}{2}n_{B-L} \ ,$$
$$n_{\bar{l}} = n_l^{eq} + \frac{1}{2}n_{B-L} \ . \tag{77}$$

These relations can be used when neglecting the influence of the sphaleron processes during the generation of the lepton asymmetry. All the different processes in thermal equilibrium during leptogenesis, such as the sphalerons, are called *spectator processes* and in this treatment these processes are neglected. Instead the sphaleron processes are considered to take place strictly after the $B-L$ asymmetry is created. Listing the reaction rates that influence the number density n_l [1]

$$\begin{aligned}\dot{n}_l + 3Hn_l = {} & \gamma(N \to l\phi) - \gamma(l\phi \to N) \\ & + \gamma(\bar{t}q \to Nl) - \gamma(Nl \to \bar{t}q) + \gamma(N\bar{t} \to l\bar{q}) \\ & - \gamma(l\bar{q} \to N\bar{t}) + \gamma(N\bar{q} \to l\bar{t}) - \gamma(l\bar{t} \to N\bar{q}) \\ & + \gamma(\bar{l}\phi^\dagger \to l\phi) - \gamma(l\phi \to \bar{l}\phi^\dagger) - \gamma(ll \to \phi^\dagger\phi^\dagger) + \gamma(\phi^\dagger\phi^\dagger \to ll) \ .\end{aligned} \tag{78}$$

Here the $\Delta L = 2$ processes $\gamma(\bar{l}\phi^\dagger \to l\phi)$, $\gamma(ll \to \phi^\dagger\phi^\dagger)$, $\gamma(l\phi \to \bar{l}\phi^\dagger)$ and $\gamma(\phi^\dagger\phi^\dagger \to ll)$, depicted in fig. 2, are now also included.

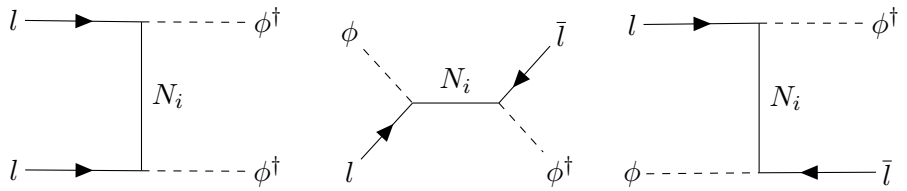

Figure 2: The $\Delta L = 2$ processes. Only the cases of a virtual intermediate N_i are considered, since real intermediate states have already been taken into account by inverse decays and subsequent decays [1].

Once again, kinetic equilibrium is assumed [1] and expressing the equation only with equilibrium reaction rates using (68), (69) and (71) gives

$$\begin{aligned}\dot{n}_l + 3Hn_l = {} & \frac{n_N}{n_n^{eq}}\gamma^{eq}(N \to l\phi) - \frac{n_l}{n_l^{eq}}\gamma^{eq}(l\phi \to N) + \frac{n_{\bar{l}}}{n_l^{eq}}\gamma^{eq}(\bar{l}\phi^\dagger \to l\phi) \\ & - \frac{n_l}{n_l^{eq}}\gamma^{eq}(l\phi \to \bar{l}\phi^\dagger) - \left(\frac{n_l}{n_l^{eq}}\right)^2 \gamma^{eq}(ll \to \phi^\dagger\phi^\dagger) + \gamma^{eq}(\phi^\dagger\phi^\dagger \to ll) \\ & + \left(1 - \frac{n_N}{n_N^{eq}}\frac{n_l}{n_l^{eq}}\right)\gamma_{\Delta L=1,s} + \left(\frac{n_N}{n_N^{eq}} - \frac{n_l}{n_l^{eq}}\right) 2\gamma_{\Delta L=1,t} \ .\end{aligned} \tag{79}$$

Using (77) to substitute n_l in (79) yields

$$\begin{aligned} & -\frac{1}{2}(\dot{n}_{B-L} + 3Hn_{B-L}) + \dot{n}_l + 3Hn_l \\ & \qquad = \frac{n_N}{n_N^{eq}}\frac{1+\varepsilon}{2}\gamma_N + \left(1 - \frac{n_N}{n_N^{eq}}\frac{(n_l^{eq} - \frac{1}{2}n_{B-L})}{n_l^{eq}}\right)\gamma_{\Delta L=1,s} \\ & \qquad + \frac{(n_l^{eq} + \frac{1}{2}n_{B-L})}{n_l^{eq}}\gamma^{eq}(\bar{l}\phi^\dagger \to l\phi) - \frac{(n_l^{eq} - \frac{1}{2}n_{B-L})}{n_l^{eq}}\gamma^{eq}(l\phi \to \bar{l}\phi^\dagger) \\ & \qquad - \left(\frac{n_l - \frac{1}{2}n_{B-L}}{n_l^{eq}}\right)^2 \gamma^{eq}(ll \to \phi^\dagger\phi^\dagger) - \frac{(n_l^{eq} - \frac{1}{2}n_{B-L})}{n_l^{eq}}\frac{1-\varepsilon}{2}\gamma_N \\ & \qquad + \left(\frac{n_N}{n_N^{eq}} - \frac{(n_l^{eq} - \frac{1}{2}n_{B-L})}{n_l^{eq}}\right) 2\gamma_{\Delta L=1,t} + \gamma^{eq}(\phi^\dagger\phi^\dagger \to ll) \ . \end{aligned} \tag{80}$$

Similarly an equation can be formulated for $n_{\bar{l}}$

$$\begin{aligned}
&\frac{1}{2}(\dot{n}_{B-L}+3Hn_{B-L})+\dot{n}_l+3Hn_l \\
&\qquad=\frac{n_N}{n_N^{eq}}\frac{1-\varepsilon}{2}\gamma_N+\left(1-\frac{n_N}{n_N^{eq}}\frac{(n_l^{eq}+\frac{1}{2}n_{B-L})}{n_l^{eq}}\right)\gamma_{\Delta L=1,s} \\
&\qquad+\frac{(n_l^{eq}-\frac{1}{2}n_{B-L})}{n_l^{eq}}\gamma^{eq}(\bar{l}\phi^\dagger\to l\phi)-\frac{(n_l^{eq}+\frac{1}{2}n_{B-L})}{n_l^{eq}}\gamma^{eq}(l\phi\to\bar{l}\phi^\dagger) \\
&\qquad-\left(\frac{n_l+\frac{1}{2}n_{B-L}}{n_l^{eq}}\right)^2\gamma^{eq}(ll\to\phi^\dagger\phi^\dagger)-\frac{(n_l^{eq}+\frac{1}{2}n_{B-L})}{n_l^{eq}}\frac{1-\varepsilon}{2}\gamma_N \\
&\qquad+\left(\frac{n_N}{n_N^{eq}}-\frac{(n_l^{eq}+\frac{1}{2}n_{B-L})}{n_l^{eq}}\right)2\gamma_{\Delta L=1,t}+\gamma^{eq}(\phi^\dagger\phi^\dagger\to ll)\ .
\end{aligned} \tag{81}$$

Subtracting (80) from (81) gives an equation for n_{B-L}. At this point it is once again useful to express the different reaction densities with the total reaction rates and the asymmetry ε as in (74). When dealing with the $\Delta L=2$ terms it is necessary to exclude the cases of a real intermediate state (RIS) from the matrix element [7, 35]. The subtracted reaction rates can be written as [1]

$$\begin{aligned}
\gamma_{sub}^{eq}(l\phi\to\bar{l}\phi^\dagger)&=\gamma_{\Delta L=2,+}+\frac{1}{2}\varepsilon\gamma_N\ , \\
\gamma_{sub}^{eq}(\bar{l}\phi^\dagger\to l\phi)&=\gamma_{\Delta L=2,+}-\frac{1}{2}\varepsilon\gamma_N\ ,
\end{aligned} \tag{82}$$

in terms of the full rate $\gamma_{\Delta L=2,+}$ and the CP asymmetry. The last terms in (80) and (81) are related with the CPT invariance and are expressed through the reaction rate [1]

$$\gamma^{eq}(ll\to\phi^\dagger\phi^\dagger)=\gamma^{eq}(\phi\phi\to\overline{ll})=\gamma_{\Delta L=2,t}\ , \tag{83}$$

so the $\Delta L=2$ reaction densities are summarised in the term [1]

$$\gamma_{\Delta L=2}=2\gamma_{\Delta L=2,+}+2\gamma_{\Delta L=2,t}\ . \tag{84}$$

Subtracting (80) from (81) and inserting (82), (83) and (84) yields

$$\begin{aligned}
\dot{n}_{B-L}+3Hn_{B-L}=&-\varepsilon\left(\frac{n_N}{n_N^{eq}}-1\right)\gamma_N \\
&-\frac{n_{B-L}}{n_l^{eq}}\left(\frac{1}{2}\gamma_N+2\gamma_{\Delta L=1,t}+\frac{n_N}{n_N^{eq}}\gamma_{\Delta L=1,s}+\gamma_{\Delta L=2}\right)\ .
\end{aligned} \tag{85}$$

The Boltzmann equations can be rewritten in a more practical form involving the reaction rates $\Gamma_{D,S,W}$ per time and particle, since comparing

these rates with the Hubble parameter H shows whether the appropriate process is in ($\Gamma_{D,S,W} > H$) or out of ($\Gamma_{D,W,S} < H$) thermal equilibrium [36]. The reaction rates and the Hubble parameter are dependent on the temperature T, however it is more convenient to work with the dimensionless parameter $z = M_1/T$, with the mass M_1 of the lightest heavy neutrino. Finally, the evolution is separated from the expansion of the universe by considering the number of particles N_x, with $x = N, B-L$, in a comoving volume space occupied by one photon and introducing the rescaled reaction rates D, S and W. The kinetic equations then read [1]

$$\frac{dN_N}{dz} = -(D+S)(N_N - N_N^{eq}) \ , \tag{86}$$

$$\frac{dN_{B-L}}{dz} = -\varepsilon D(N_N - N_N^{eq}) - W N_{B-L} \ . \tag{87}$$

For more details on the calculations see appendix C.

The dynamics of N production is determined by the decay rate D and the scattering rate S and depends on the deviation of N_N from the equilibrium number N_N^{eq}. The evolution of the $B-L$ asymmetry is governed by two competing terms. It is also generated through the difference between N_N and N_N^{eq} and directly proportional to the CP asymmetry ε. The washout processes W on the other hand reduce N_{B-L}. Leptogenesis depends on the neutrino parameters such as the light neutrino masses $m_{1,2,3}$, the heavy neutrino mass M_1 and the effective neutrino mass

$$\tilde{m}_1 = \frac{(m_D^\dagger m_D)_{11}}{M_1} \ , \tag{88}$$

with the Dirac mass matrix m_D from (44). The different reaction rates D, S and W depend on $\tilde{m}_1$ [7, 37], which thus defines the regions of z in which these reactions are in or out of thermal equilibrium. It allows for a convenient definition of the decay parameter introduced in ordinary GUT baryogenesis [36]

$$K = \frac{\Gamma_D(z=\infty)}{H(z=1)} = \frac{\tilde{m}_1}{m_*} \ , \tag{89}$$

comparing $\tilde{m}_1$ to the equilibrium mass m_*

$$m_* = \frac{16\pi^{5/2}\sqrt{g_*}}{3\sqrt{5}} \frac{v^2}{M_{\rm Pl}} \simeq 1.08 \cdot 10^{-3}\,{\rm eV} \ , \tag{90}$$

where $g_* = 106.75$ resembles the total number of degrees of freedom and $M_{\rm Pl} = 1.22 \cdot 10^{19}\,{\rm GeV}$ is the Planck mass [2]. This separates two regimes. The weak washout regime is defined by $K < 1$, which means that the relevant processes do not go into thermal equilibrium. Vice versa, a value of $K > 1$ marks the strong washout regime where the processes reach thermal

equilibrium [7]. Fig. 3a and fig. 3b illustrate the evolution of the N and $|N_{B-L}|$ abundance with z in the weak and the strong washout regime respectively. They also compare the effects of different initial conditions N_N^i and show the evolution with and without including the $\Delta L = 1$ and $\Delta L = 2$ processes. The plots have been created with `ULYSSES` as described in section 5.3.

In all scenarios N_N^{eq} and N_N drop off for large values of z and the N production will eventually be kinematically suppressed. Then, the generation of the $B - L$ asymmetry will freeze out and reach a final value [1]

$$N_{B-L}^f = N_{B-L}(z = \infty) = -\frac{3}{4}\varepsilon\kappa_f \ , \tag{91}$$

with the efficiency factor $\kappa(z)$ and its final value κ_f. In the weak washout regime, as shown in fig. 3a, N_{B-L}^f depends on the initial conditions. For thermal initial abundance $N_N^i = 3/4$, $N_N > N_N^{eq}$ for all z and $|N_{B-L}|$ is monotonically increasing, whereas if $N_N^i = 0$, so for zero initial abundance, $N_N < N_N^{eq}$ at first until z reaches the value z_{eq} where $N_N(z_{eq}) = N_N^{eq}(z_{eq})$. This leads to the brief drop of the $|N_{B-L}|$ curve. κ_f and therefore $|N_{B-L}|$ is proportional to N_N^i up to first order in K, which is why the thermal initial condition leads to a larger final value. Including scatterings and $\Delta L = 2$ processes primarily enhances the washout and the production of N_N for $z < z_{eq}$ and zero initial abundance. Since the number of decaying particles is larger, the final value of $|N_{B-L}|$ is enhanced as well. Thus, in the weak washout regime, the results are highly dependent on the initial conditions. In the strong washout regime however, as depicted in fig. 3b, the decay gets into thermal equilibrium. Because of this, $z_{eq} < 1$ and the N abundance tracks the equilibrium value already at higher temperatures. Also the washout processes get into and eventually out of thermal equilibrium, which reduces $|N_{B-L}|$ in some z region. Because of this, thermal and zero initial abundance are practically equivalent concerning $|N_{B-L}^f|$ and the strong washout regime does not depend on the initial conditions or any hypothetical previous $B-L$ generating mechanism [7].

The baryon to photon ratio can be expressed using N_{B-L}^f [1]

$$\eta_B = \frac{c_S}{f}|N_{B-L}^f| = \frac{3}{4}\frac{c_S}{f}\varepsilon\kappa_f \simeq 0.96 \cdot 10^{-2}\varepsilon\kappa_f \ . \tag{92}$$

The factor 3/4 arises from Fermi statistics which, together with the CP asymmetry ε, describes the final value only considering decays and inverse decays. The influence of the sphaleron processes is described with the number c_S from (23) and $f = 2387/86$ deals with the increasing amount of photons in the comoving volume space. The efficiency factor κ then includes the other interactions with the thermal bath and different possible initial conditions. Its precise value has to be calculated from the differential equations [1].

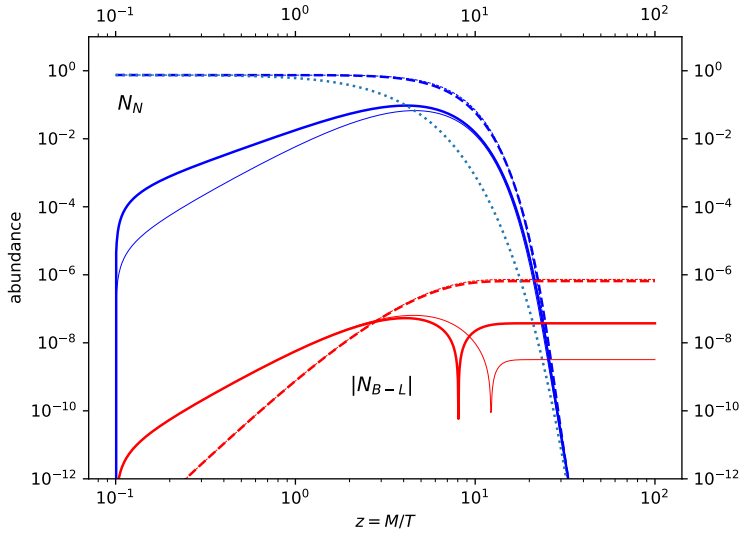

(a)

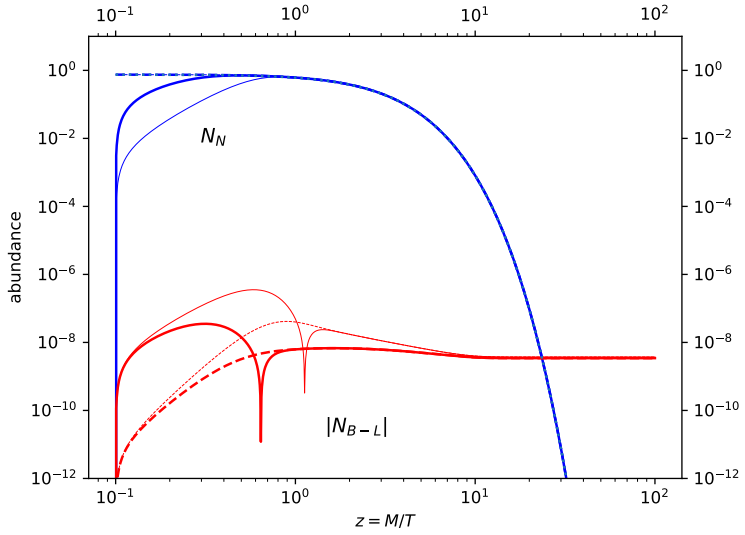

(b)

Figure 3: The evolution of the N (blue) and $B-L$ (red) abundances with z. The solid lines correspond to $N_N^i = 0$, the dashed lines to $N_N^i = 3/4$. The thin lines mark the case of just decays and inverse decays whereas the thick lines include $\Delta L = 1, 2$ processes. The light blue dotted line describes the evolution of N_N^{eq}. The plots show NO with masses $M_1 = 10^{14}\,\text{GeV}$, $m_1 = 0\,\text{eV}$. Fig. 3a resembles the weak washout regime with $K = 10^{-97}$, fig. 3b shows the strong washout regime with $K = 45$. The plots are designed to resemble the figures in [34] in order to emphasise the capabilities of `ULYSSES`.

4.3 Rescaled reaction rates

In order to proceed one can solve the equations (86) and (87) numerically with a program such as `ULYSSES` or, alternatively, try to find analytical approximations like in [7]. Either way it is necessary to formulate approximated terms for the rates D, S and W as well as N_N^{eq} and N_l^{eq} dependent on z and the neutrino parameters to then work with. Starting with the decay rate [38, 39]

$$D(z) = Kz \left\langle \frac{1}{\gamma} \right\rangle = Kz \frac{K_1(z)}{K_2(z)} \ , \tag{93}$$

with the thermally averaged dilation factor $\left\langle \frac{1}{\gamma} \right\rangle$ which is expressed with the modified Bessel functions $K_1(z)$ and $K_2(z)$. The equilibrium numbers of the decaying heavy neutrino N_N^{eq} and the leptons N_l^{eq} read [7]

$$N_N^{eq}(z) = \frac{3}{8} z^2 K_2(z) \quad , \quad N_l^{eq} = \frac{3}{4} \ . \tag{94}$$

The following derivations of the scattering and washout terms are taken from [7]. The scattering rate S is described with the processes involving the top quark S^t as depicted in fig. 1 and is split into the contributions from the s- and t-channel

$$S^t = 2S_{\phi,s} + 4S_{\phi,t} \ . \tag{95}$$

From evaluating the reaction rate densities one can find

$$S^t = \frac{K_S}{6} (f_{\phi,s}(z) + 2 f_{\phi,t}(z)) \ , \tag{96}$$

with $K_S = \tilde{m}_1 / m_*^s$ and

$$m_*^s = \frac{4\pi^2}{9} \frac{g_N v^2}{m_t^2} m_* \simeq 10 m_* \ , \tag{97}$$

where $g_N = 2$ is the number of degrees of freedom of the heavy Majorana neutrino. For $z \ll 1$ the functions $f_{\phi,s}(z)$ and $f_{\phi,t}(z)$ are approximated as

$$\begin{aligned} f_{\phi,s}(z) &\simeq 2 \left[1 - z^2 \left(\ln \left(\frac{2}{z} \right) \right) - \gamma_E \right] \ , \\ f_{\phi,t}(z) &\simeq 2 \left[1 + \frac{z^2}{2} \ln \left(\frac{M}{M_h} \right) \left(\ln \left(\frac{2}{z} \right) \right) - \gamma_E \right] \ , \end{aligned} \tag{98}$$

with the Higgs mass M_h. For the Boltzmann equations the sum $D + S$ is relevant. It is approximated as

$$D + S \simeq K_S \left[1 + \ln \left(\frac{M}{M_h} \right) z^2 \ln \left(1 + \frac{a}{z} \right) \right] \ , \tag{99}$$

where

$$a = \frac{K}{K_S \ln\left(M/M_h\right)} \ . \tag{100}$$

The total washout W is separated into two parts which are only dependent on $\tilde{m}_1$ and the product $M_1\overline{m}$

$$W(z; \tilde{m}_1, M\overline{m}^2) = W_0(z; \tilde{m}_1) + \Delta W(z; M\overline{m}^2) \ , \tag{101}$$

where $\overline{m} = \sqrt{m_1^2 + m_2^2 + m_3^2}$ is the light neutrino mass scale. W_0 itself consists of the contribution from inverse decays W_{ID} and $\Delta L = 1$ scattering $W_{\Delta L=1}$. The inverse decay rate Γ_{ID} is related to the decay rate Γ_D via

$$\Gamma_{ID}(z) = \Gamma_D(z) \frac{N_N^{eq}}{N_l^{eq}} \ . \tag{102}$$

Going to the rescaled inverse decay rate using (93) and (94) gives

$$W_{ID} = \frac{1}{2}\frac{\Gamma_{ID}}{Hz} = \frac{1}{2} D(z) \frac{N_N^{eq}(z)}{N_l^{eq}} = \frac{1}{4} K z^3 K_1(z) \ . \tag{103}$$

A similar relation as in (102) can be used in order to connect $W_{\Delta L=1}$, which again is described with a s- and a t-channel

$$W_{\Delta L=1} = W_{\phi,s} + 2W_{\phi,t} \ , \tag{104}$$

to the appropriate scattering rates

$$W_{\phi,t} = \frac{N_N^{eq}}{N_l^{eq}} S_{\phi,t} \ ,$$

$$W_{\phi,s} = \frac{N_N^{eq}}{N_l^{eq}} \frac{N_N}{N_N^{eq}} S_{\phi,s} \ . \tag{105}$$

With (103), (104) and (105) $W_{\Delta L=1}$ is expressed in terms of W_{ID} and D. Then, $W_0 = W_{ID} + W_{\Delta L=1}$ takes the form

$$W_0 = W_{ID} \left(1 + \frac{1}{D}\left(2\frac{N_N}{N_N^{eq}} S_{\phi,s} + 4S_{\phi,t}\right)\right) \ . \tag{106}$$

In the case of dynamical initial N abundance at high temperatures, (106) is approximated with $N_N/N_N^{eq} \simeq 0$ and therefore

$$W_0 \simeq W_{ID}(z) \frac{D + 4S_{\phi,t}}{D} \simeq W_{ID}\left(1 + \frac{\alpha}{z}\right) \ , \tag{107}$$

with

$$\alpha = \frac{2K_S}{3K} + \frac{15}{8} \ . \tag{108}$$

On the other hand, for thermal initial abundance or in the strong washout regime, N_N tracks closely to N_N^{eq}, which enables the approximation $N_N/N_N^{eq} \simeq 1$. With (99) this yields

$$W_0 \simeq W_{ID}(z)\frac{D+S}{D} \simeq W_{ID}(z)\left[\frac{z}{a}\ln\left(1+\frac{a}{z}\right)+\frac{K_S}{Kz}\right]\left(1+\frac{15}{8z}\right) \ . \quad (109)$$

ΔW is given by the $\Delta L = 2$ processes and at low temperatures it is approximated as

$$\Delta W \simeq \frac{\omega}{z^2}\left(\frac{M}{10^10\,\mathrm{GeV}}\right)\left(\frac{\overline{m}}{\mathrm{eV}}\right)^2 \ , \quad (110)$$

with the constant ω

$$\omega = \frac{9\sqrt{5}M_{\mathrm{Pl}}10^{-8}\mathrm{GeV}^3}{4\pi^{9/2}g_l\sqrt{g_*}v^4} \simeq 0.186 \ . \quad (111)$$

With this, D, S and W are all expressed in terms of the well known Bessel functions $K_1(z)$ and $K_2(z)$.

4.4 Evolution of κ_f

The general solution to the equation (87) describing the evolution of N_{B-L} is [36]

$$N_{B-L}(z) = N^i_{B-L}e^{-\int_{z_i}^{z}dz'W(z')} - \frac{3}{4}\varepsilon\kappa(z) \ , \quad (112)$$

with κ [7]

$$\kappa(z) = -\frac{4}{3}\int_{z_i}^{z}dz'\frac{D}{D+S}\frac{dN_N}{dz'}e^{-\int_{z'}^{z}dz''W(z'')} \ . \quad (113)$$

The problem is now to find a value for κ or, more specifically, κ_f.

The numerical solution from `ULYSSES` is depicted in Fig. 4, which shows the evolution of κ_f with $\tilde{m}_1$. In the weak washout regime κ_f is proportional to $(4/3)N_N^i$ in first order of $\tilde{m}_1$, leading to $\kappa_f = 1$ for thermal initial abundance. In the case of zero initial abundance, the non zero value of κ_f is obtained by including the washout processes. For this scenario the efficiency factor can be split at z_{eq} into κ^-, a negative contribution where inverse decays dominate, and a positive contribution κ^+, where decays dominate. The final efficiency factor κ_f is given by the sum $\kappa_f = \kappa_f^- + \kappa_f^+$. The washout then reduces κ_f^-, thus leading to an enhanced κ_f in $\mathcal{O}(\tilde{m}_1^2)$. So, with rising $\tilde{m}_1$ the contribution of the washout and therefore κ_f increases. Taking into account the scattering enhances the number of decaying particles in the weak regime even further, as already depicted in fig. 3a and fig. 3b, which in turn also increases κ_f. Also, for thermal initial abundance κ_f is slightly reduced when including the $\Delta L = 1$ scatterings to the washout. In the strong washout regime the washout processes go into thermal equilibrium in a temperature region $z_{\mathrm{in}} < z < z_{\mathrm{out}}$, which leads to a reduction of κ_f.

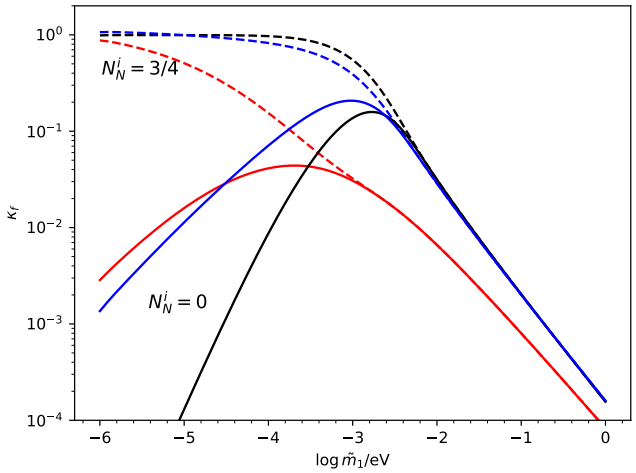

Figure 4: The final efficiency factor κ_f as a function of $\tilde{m}_1$. The plot is created for NO with $m_1 = 0\,\mathrm{eV}$ and $M_1 = 10^{14}\,\mathrm{GeV}$. The black lines only consider decays and inverse decays, the blue lines include $\Delta L = 1$ scattering and the red lines also consider $\Delta L = 2$ processes. The solid lines are for $N_N^i = 0$, the dashed ones represent $N_N^i = 3/4$. The plot is created using `ULYSSES` as described in section 5.3.

Any asymmetry for $z < z_{\mathrm{in}}$ is washed out. Because of this, the course of the curves for thermal and zero initial abundance is equal in this regime and κ_f is independent of the initial conditions. For the here displayed set of neutrino parameters there is no visible difference between only considering decays and inverse decays and also taking $\Delta L = 1$ scatterings into account. The $\Delta L = 2$ washout is included by adding the approximated washout term ΔW from (110) to the total washout. Since the washout is enhanced, κ_f is once again increased for zero initial abundance in the weak washout regime, for the case of thermal initial abundance and in the strong washout regime the final efficiency factor is reduced. Notably ΔW is a function of the product $M\overline{m}^2$ and not proportional to $\tilde{m}_1$ [7].

4.5 Deriving neutrino mass bounds

Leptogenesis can be used in a very straightforward way to obtain bounds on the light neutrino masses $m_{1,2,3}$ and the lightest heavy RHN mass M_1, by simply calculating a maximal baryon to photon ratio $\eta_B^{\max}$ and comparing it to the measured value $\eta_B^{\mathrm{CMB}} = (6.12 \pm 0.04) \cdot 10^{-10}$ from experiment [6, 7]. This yields a condition

$$\eta_B^{\mathrm{CMB}} \leq \eta_B^{\max} \ , \tag{114}$$

which in turn is used to impose boundaries on the masses. In general, the CP asymmetry ε can be expressed with a maximal value $\varepsilon^{\max}$ and an effective leptogenesis phase δ_L as [40]

$$\varepsilon = \varepsilon^{\max} \sin \delta_L \ . \tag{115}$$

Taking just $\varepsilon^{\max}$ and determining κ_f by calculating it numerically with ULYSSES gives an expression for $\eta_B^{\max}$ [1, 7]

$$\eta_B^{\max} \simeq 0.96 \cdot 10^{-2} \varepsilon^{\max} \kappa_f \ . \tag{116}$$

$\varepsilon^{\max}$ and κ_f only depend on the different mass terms M_1, $\tilde{m}_1$ and the lightest light neutrino mass m. It is beneficial to split $\varepsilon^{\max}(M_1, \tilde{m}_1, m_1)$ into two factors to separate the mass dependencies [6]

$$\varepsilon^{\max}(M_1, \tilde{m}_1, m) = \varepsilon'(M) \beta(\tilde{m}_1, m_1) \ , \tag{117}$$

where $\varepsilon'(M_1)$ corresponds to $\varepsilon^{\max}(M_1, \tilde{m}_1, m_1)$ in the limit $m = 0\,\text{eV}$ and $\tilde{m}_1 \to \infty$ and it reads [41]

$$\varepsilon'(M_1) = \frac{3}{16\pi} \frac{M_1 m_{\text{atm}}}{v^2} \simeq 10^{-6} \left(\frac{M_1}{10^{10}\,\text{GeV}} \right) \left(\frac{m_{\text{atm}}}{0.05\,\text{eV}} \right) \ , \tag{118}$$

with $m_{\text{atm}} = \sqrt{\Delta m^2_{\text{atm}}}$, which leads to different values for NO and IO. $\beta(\tilde{m}_1, m_1)$ is once again split into $\beta_{\max}(m)$ and $f(\tilde{m}_1, m)$ [7]. The first factor needs to fulfil $\beta_{\max}(m) = 1$ for $m = 0\,\text{eV}$ and suppresses ε for larger m. It reads [7]

$$\beta_{\max}(m) = \frac{m_{\text{atm}}}{m' + m} = \frac{m' - m}{m_{\text{atm}}} \ , \tag{119}$$

where m' is the largest light neutrino mass, so $m' = m_3$ for NO and $m' = m_2$ for IO. The dependence on $\tilde{m}_1$ is then located in $f(\tilde{m}_1, m)$, which is expressed as [7]

$$f(\tilde{m}_1, m) = \frac{m' - m\sqrt{1 + \frac{m^2_{\text{atm}}}{\tilde{m}_1^2}}}{m' - m} \ . \tag{120}$$

For $m = 0\,\text{eV}$, the function $f(\tilde{m}_1, m) = 1$ independently of $\tilde{m}_1$. The effective neutrino mass is constrained by $\tilde{m}_1 \geq m$ [42]. For $\tilde{m}_1 \gtrsim m$, $f(\tilde{m}_1, m)$ becomes small and suppresses $\varepsilon^{\max}$, while for $\tilde{m}_1 \gg m$, $f(\tilde{m}_1, m)$ approaches 1 [6].

5 Numerical analysis

5.1 The ULYSSES program

ULYSSES is the first publicly available python package dedicated to determining η_B from leptogenesis in the context of a type-I seesaw mechanism [4,

5]. It is written in python3 and uses NUMPY [43, 44] and SCIPY [45], as well as ODEINTW [46] for solving the coupled differential equations. The calculation is accelerated with NUMBA [47]. The code is structured in a way that the general infrastructure of the calculation is contained in a base class. This includes setting the global variables, parameterising the Yukawa and the PMNS matrix and defining terms for the CP asymmetries and reaction rates. The base class works with a dummy function EtaB, which has to be overwritten with a separate plugin. This plugin defines the actual Boltzmann equations. Thus, it is easy to implement different leptogenesis models by simply changing the plugin. Overall, `ULYSSES` is supposed to be a fast and flexible code which can be easily modified and therefore further developed [4].

In the base function `uls-base` the reaction rates D, $D+S$, W_{ID}, $(D+S)/D$ and N_N^{eq} are defined as in section 4.3 with (93), (99), (103), (109) and (94) respectively. The matrix U_{PMNS}, which is used to describe neutrino mixing, is defined with (28). To describe the Yukawa matrix Y, the relation with the neutrino Dirac mass matrix $m_D = Yv$ and the Casas-Ibarra parameterisation from (54) is used, which yields [4]

$$Y = \frac{1}{v} U_{\text{PMNS}} \sqrt{\hat{m}} R^T \sqrt{\hat{M}} \tag{121}$$

in the flavour basis. The remaining free parameters of Y make up the required input parameters of `ULYSSES`. U_{PMNS} contributes the mixing angles θ_{12}, θ_{13}, θ_{23}, the CP violating phase δ and the Majorana phases α_{21} and α_{31} as first six parameters. Another six are added in the form of the complex angles $\omega_j = x_j + iy_j$, where $j = 1, 2, 3$, for the orthogonal matrix R. Lastly, there are the heavy neutrino masses $M_{1,2,3}$ and the lightest light neutrino mass m. The remaining light neutrino masses are determined with the solar and atmospheric mass squared splittings, where `ULYSSES` takes the central values of NuFIT 5.1 data [27] as presented in (35) and (36). `ULYSSES` can switch between NO and IO by a command line input. Alternatively it is also possible to set the individual entries of the Yukawa matrix directly by providing a magnitude and a phase value for each one, which leads to 21 input parameters instead of the above stated 16.

`ULYSSES` and the extended `ULYSSES` version 2 already come with a series of plugins for Boltzmann equations for different physical scenarios as well as four different runtime scripts. The script `uls-calc` evaluates just one point in the parameter space and returns a value for the final value of η_B, together with the corresponding values of the baryonic yield Y_B and the baryonic density parameter Ω_B [4]

$$Y_B = \eta_B \frac{45\zeta(3)}{\pi^4 g_{*,s}(t_{\text{rec}})} \quad , \quad \Omega_B h^2 = \eta_B \frac{m_p n_\gamma}{\rho_c h^{-2}} \ , \tag{122}$$

with the entropic degrees of freedom at present $g_{*,s}(t_{\text{rec}}) = 43/11$, the proton mass m_p and the critical density of the universe. Another output of this

script is $|N_{B-L}|$ and η_B as a function of the evolution parameter z. The other three scripts are used for multi-dimensional analyses of the parameter space. With `uls-scan` and `uls-scan2D` one can generate plots or text files with the calculated data for the final value of η_B as a function of one or two of the input parameters in a set range. In order to investigate a higher dimensional parameter space, `uls-nest` can be used. This script makes use of MULTINEST [48] and scans a given parameter space to find regions with a value of η_B with maximum likelihood compared to a reference value from experiment. For this, a simple log-likelihood is implemented [4]. The module `slc-scan2D` is used for the main analysis as described in section 5.3. Additionally, fig. 3a and fig. 3b were created using `uls-calc`, which enables to access the output for different values of the evolution parameter z. The module `uls-scan` was used for fig. 4.

`ULYSSES` provides built-in plugins for semi classical Boltzmann equations neglecting flavour effects as well as two- and three-flavoured Boltzmann equations for one and two decaying RHNs respectively. This already includes the simplest case of thermal leptogenesis as presented in (86) and (87), neglecting the scattering rate S. Additionally, there are models that include density matrix equations for one, two and three decaying RHNs respectively, which account for off-diagonal flavour oscillations. There is one script which adds $\Delta L = 1$ scattering effects to the density matrix equation of three decaying RHNs. Another analyses the evolution of the simplest case of thermal leptogenesis regarding the scale factor a instead of z. The last plugins of `ULYSSES` version 1 investigate the three-flavoured Boltzmann equation for the decay of two RHNs in the resonant case with and without spectator processes up to $T \ll 10^8\,\mathrm{GeV}$ [4]. For the decay of one RHN in the single flavour approximation Maxwell Boltzmann statistics and kinetic equilibrium are assumed, as discussed in section 4. `ULYSSES` version 2 introduces three new cases which allow to drop those assumptions independently. It also features a plugin for the Akhmedov-Rubakov-Smirnov (ARS) mechanism for leptogenesis and for analysing the possible effects of evaporating primordial black holes on leptogenesis [5].

5.2 Adjusted plugin

This work deals with the case of one decaying RHN in the single flavour approximation, taking into account $\Delta L = 1$ scatterings and $\Delta L = 2$ processes. Therefore, the plugin `1BE1F`, provided by `ULYSSES`, is used as a starting point, as this also includes only one decaying RHN in the single flavour approximation and comes closest to the desired application. The full code of the `1BE1F` plugin from `etaB1BE1F.py` is shown in appendix D. This plugin implements the Boltzmann equations from (86) with $S = 0$

$$\frac{dN_N}{dz} = -D(N_N - N_N^{eq}) \ ,$$

```
def fast_RHS(y0, ds, w1, n1eq, epstt,epsmm,epsee, d):

    N1      = y0[0]
    NBL     = y0[1]

    rhs1 =                          -ds*(N1-n1eq)

    rhs2 =    (epstt+epsmm+epsee)*d*(N1-n1eq)-w1*NBL

    return [rhs1, rhs2]
```

Listing 1: Redefiniton of the Boltzmann equations now featuring scattering via `ds` in `rhs1`, which represents $D + S$.

```
            #definitions of D+S, D, W and N^eq
            self._ds      = np.real(self.DS(k,z))
            self._d    = np.real(self.D1(k,z))
            self._w1     = self.scat(z)*np.real(self.W1(k, z))
   +(0.186/z**2)*(self.M1*1e-10)*(mbar*1e9)**2 #strong washout
    w0=wID*j + DeltaL=2
            self._n1eq    = self.N1Eq(z)
            self._currz=z
```

Listing 2: Inclusion of $\Delta L = 2$ washout with the additional term in `self._w1`.

and (87)

$$\frac{dN_{B-L}}{dz} = -\varepsilon D(N_N - N_N^{eq}) - W_{ID} N_{B-L} \ ,$$

only including the contribution of inverse decays to the washout rate W. The provided plugin `3DMEsct` is used as a reference to implement the $\Delta L = 1$ scattering, as this already uses the scattering terms as presented in 4.3. The implementation of the Boltzmann equations can be changed immediately to include $D + S$, as displayed in listing 1.

As shown in (101), the washout rate is described with the two parts W_0 and ΔW. The code for W_0 is adopted from `3DMEsct`. To also take the $\Delta L = 2$ processes into account, the approximation (110) is added as well. The adjusted code is shown in listing 2.

The final change is made to the definition of the CP asymmetry. `ULYSSES` defines the asymmetry as $\varepsilon = \varepsilon_{ee} + \varepsilon_{\mu\mu} + \varepsilon_{\tau\tau}$. Since the decay of only one RHN is discussed, only one parameter is relevant. Listing 3 shows how this one is then defined as $\varepsilon^{\max}$ from (117), while the others are set to zero. Furthermore, the functions $\beta_{\max}$ and f are included as presented in (119) and (120) respectively.

The equations used in these adjustments are taken from [7], where a different notation to the rest of `ULYSSES` was used for the light neutrino

```
        #setting mass dependent maximal espilon
        beta_max=np.sqrt(self.msplit2_athm_normal)/(m3+m1)
        sqrt=np.sqrt(1+self.msplit2_athm_normal/np.square(self.
meff1))
        f=(m3-m1*sqrt)/(m3-m1)

        epstt = 0
        epsmm = 0
        epsee = np.real((3*self.M1*np.sqrt(self.
msplit2_athm_normal))/(16*np.pi*np.square(self.v)))*
beta_max*f
```

Listing 3: Definition of ε together with the functions $\beta_{\max}$ and f.

```
            #definition of masses for NO
            m1=self.m
            m2=np.sqrt(self.msplit2_solar + self.m*self.m)
            m3=np.sqrt(self.msplit2_athm_normal + self.m*self.m
)
            mbar=np.sqrt(np.square(m1)+np.square(m2)+np.square(
m3))
```

Listing 4: Definition of `m1`, `m2` and `m3` in NO

masses. With this notation, $m_{1,2,3}$ refer to the lightest, intermediate and the heaviest light neutrino masses respectively instead of the neutrino mass eigenstates. For simplicity, the equations were not changed but instead the masses are redefined in the new plugin in both functions EtaB and RHS to fit this mass pattern. Thus, there are two different plugins for NO and IO. The relevant code lines are shown in listing 4 for NO and in listing 5 for IO.

Now the code is modified to return the final value of $\eta_B^{\max}$ for a given set of M_1, $\tilde{m}_1$ and m.

M_1 and m are input parameters and can be set directly with `ULYSSES`, other than $\tilde{m}_1$, which needs to be constructed first. The effective mass is defined as in (88). Using $m_D = Yv$, the effective mass can be expressed

```
            #definition of masses for IO
            m2=np.sqrt(self.msplit2_athm_invert + self.m*self.m
 - self.msplit2_solar)
            m3=np.sqrt(self.msplit2_athm_invert + self.m*self.m
)
            m1=self.m
            mbar=np.sqrt(np.square(m1)+np.square(m2)+np.square(
m3))
```

Listing 5: Definition of `m1`, `m2` and `m3` in IO

```
            self._w1     = self.scat(z)*np.real(self.W1(k, z))
    +(0.186/z**2)*(M[0,0]*1e-10)*(np.sqrt(self.msplit2_solar+2*
    self.msplit2_athm_normal)*1e9)**2 #strong washout w0=wID*j+
    DeltaL=2
```

Listing 6: Full washout term for fixed $m = 0\,\text{eV}$ for NO

```
        #eps_max for lightest small neutrino mass m=0
        epstt = 0
        epsmm = 0
        epsee = np.real((3*self.M1*0.05*1e-9)/(16*np.pi*np.
    square(self.v)))
```

Listing 7: ε for fixed $m = 0\,\text{eV}$ for NO

through Y

$$\tilde{m}_1 = \frac{(m_D^\dagger m_D)_{11}}{M_1} = \frac{v^2 (Y^\dagger Y)_{11}}{M_1} \ . \tag{123}$$

The definition of the Yukawa matrix in the Casas-Ibarra parameterisation (13) gives for

$$(Y^\dagger Y)_{ij} = \frac{1}{v^2} \sum_b (R^*)_{ib} m_b (R^T)_{bj} \sqrt{M_i M_j} \ , \tag{124}$$

where m_b and $M_{i,j}$ are the light and heavy neutrino masses respectively. Including the explicit values for the orthogonal matrix R this then leads to

$$\tilde{m}_1 = \sum_b |R_{1b}|^2 m_b = m_1 |c_{\omega_2} c_{\omega_3}|^2 + m_2 |c_{\omega_2} s_{\omega_3}|^2 + m_3 |s_{\omega_2}|^2 \ , \tag{125}$$

with $c_{\omega_j} = \cos\omega_j$, $s_{\omega_j} = \sin\omega_j$ and $\omega_j = x_j + i y_j$ as in section 3.2. Now it is possible to vary $\tilde{m}_1$ with the input parameters. $\tilde{m}_1$ is independent of the complex angle ω_1 and determined by x_2, y_2, x_3 and y_3. In a simplified picture one can choose $x_3 = y_3 = y_2 = 0°$ and $x_2 = 0°$ or $x_2 = 90°$ for NO and IO respectively, such that in both cases $\tilde{m}_1 = m$. Then, the Boltzmann equations can be fixed to $m = 0\,\text{eV}$ by setting

$$\varepsilon(M, \tilde{m}_1, m) = \varepsilon'(M) \ , \tag{126}$$

as in (118) and fixing

$$\overline{m} = \sqrt{\Delta m^2_{\text{atm}} + \Delta m^2_{\text{sol}}} \ . \tag{127}$$

These two adjustments are displayed in listing 6 and in listing 7 for NO.

This way, the physical scenarios are limited to the case $m = 0\,\text{eV}$ and $\tilde{m}_1$ is identical with the input of m. This simple picture was used for fig. 3 and fig. 4.

To instead change $\tilde{m}_1$ for a fixed $m \neq 0\,\mathrm{eV}$, the complex angles $\omega_{1,2}$ have to be used as variables in the parameter scan. Three of the angle components can be fixed to simplify the equation. Either one of the imaginary parts $y_{2,3}$ should be chosen as the evolution parameter, as they are the argument of hyperbolic functions which are not bounded. First consider NO with $m = m_1$. Since $\tilde{m}_1 \geq m_1$ [42] and $m_1 < m_{2,3}$, the parameters should be chosen in a way that m_1 is connected to the arising cosh term. Setting $x_2 = y_2 = x_3 = 0°$ then leads to

$$\tilde{m}_1^{\mathrm{NO}} = m_1 \cosh^2(y_3) + m_2 \sinh^2(y_3) \ . \tag{128}$$

For IO, the parameters are chosen as $x_2 = 90°$, $x_3 = y_3 = 0°$, which yields

$$\tilde{m}_1^{\mathrm{IO}} = m_1 \sinh^2(y_2) + m_3 \cosh^2(y_2) \ . \tag{129}$$

5.3 Numerical results

First, the parameter region is analysed for NO. The 2 dimensional parameter scans are conducted with the application `uls-scan2D`. In NO the lightest light neutrino mass is the mass eigenstate m_1, which then corresponds to the input parameter m. The masses m_2, m_3 are determined with (34) and (35)

$$\begin{aligned} m_2 &= \sqrt{m^2 + \Delta m^2_{\mathrm{sol}}} \ , \\ m_3 &= \sqrt{m^2 + (\Delta m^{\mathrm{NO}}_{\mathrm{atm}})^2} \ , \end{aligned} \tag{130}$$

where $m^2_{\mathrm{sol}} = 7.420 \cdot 10^{-5}\,\mathrm{eV}^2$ and $(\Delta m^{\mathrm{NO}}_{\mathrm{atm}})^2 = 2.515 \cdot 10^{-3}\,\mathrm{eV}^2$ [27]. The mass scale then reads

$$\overline{m} = \sqrt{3m^2 + \Delta m^2_{\mathrm{sol}} + (\Delta m^{\mathrm{NO}}_{\mathrm{atm}})^2} \ . \tag{131}$$

N^i_N is set to zero. The heavy neutrino mass M_1 varies from 10^8 to $10^{16}\,\mathrm{GeV}$. The second variable that is changed during the scan is y_3 which goes from $0°$ up to $250°$. As described above, $x_2 = x_3 = y_2 = 0°$, such that

$$\tilde{m}_1^{\mathrm{NO}} = m \cosh^2(y_3) + \sqrt{m^2 + \Delta m^2_{\mathrm{sol}}} \sinh^2(y_3) \ . \tag{132}$$

Both parameters are scanned for 100 equally distanced values, creating a 100×100 grid for the results η_B. The values y_3 are converted into $\tilde{m}_1$ using (132), which causes the parameter grid to be deformed. There are very few data points in the weak washout region $\tilde{m}_1 \lesssim 10^{-3}$. To enhance the numerical accuracy in that region, an additional scan is performed in a more restricted region of y_3 from $0°$ to $10°$, which covers $\tilde{m}_1$ up to $\mathcal{O}(10^{-4})\,\mathrm{eV}$. In fig. 5a the results for η_B in the ($\tilde{m}_1$-M_1)-plane are compared to the lower 3σ region of $\eta_B^{\mathrm{CMB}} = (6.12 \pm 0.04) \cdot 10^{-10}$, resulting in an allowed region for

a fixed value of m. Multiple scans are conducted for increasing values of m. It is observed that the allowed region shrinks and for $m = 0.119\,\mathrm{eV}$ it vanishes completely which therefore translates to the upper bound

$$m_1 < 0.119\,\mathrm{eV}\ . \tag{133}$$

This is the method of analysis used in [6]. The appropriate bounds for m_2 and m_3 follow from (130)

$$m_2 < 0.119\,\mathrm{eV} \quad , \quad m_3 < 0.129\,\mathrm{eV}\ . \tag{134}$$

The mass scale is bounded by

$$\overline{m} < 0.212\,\mathrm{eV}\ . \tag{135}$$

In the case of IO, the same method is used however some parameters have to be chosen differently. The input m is now the mass eigenstate m_3, as this is the lightest light neutrino mass for IO. The solar mass splitting remains the same, but the atmospheric mass splitting has a different value $(\Delta m^{2\,\mathrm{NO}}_{\mathrm{atm}})^2 = 2.498 \cdot 10^{-3}\,\mathrm{eV}^2$ [27]. The masses m_1 and m_2 are calculated according to

$$\begin{aligned} m_1 &= \sqrt{m^2 + (\Delta m^{2\,\mathrm{IO}}_{\mathrm{atm}})^2 - \Delta m^2_{\mathrm{sol}}}\ , \\ m_2 &= \sqrt{m^2 + (\Delta m^{2\,\mathrm{IO}}_{\mathrm{atm}})^2}\ , \end{aligned} \tag{136}$$

while the mass scale reads

$$\overline{m} = \sqrt{3m^2 - \Delta m^2_{\mathrm{sol}} + 2(\Delta m^{2\,\mathrm{IO}}_{\mathrm{atm}})^2}\ . \tag{137}$$

Now the angle parameters are chosen as $x_3 = y_3 = 0°$ and $x_2 = 90°$, such that $\tilde{m}_1$ is defined as

$$\tilde{m}_1^{\mathrm{IO}} = m \cosh^2(y_2) + \sqrt{m^2 + (\Delta m^{2\,\mathrm{IO}}_{\mathrm{atm}})^2 - \Delta m^2_{\mathrm{sol}}}\, \sinh^2(y_2)\ , \tag{138}$$

y_2 is the varied input parameter. As depicted in fig. 5b the allowed region vanishes for $m = 0.117\,\mathrm{eV}$ so that the upper bound on m_3 reads

$$m_3 < 0.117\,\mathrm{eV}\ . \tag{139}$$

With (136) the other masses are restricted to

$$m_1 < 0.127\,\mathrm{eV} \quad , \quad m_2 < 0.127\,\mathrm{eV}\ , \tag{140}$$

the mass scale is limited to

$$\overline{m} < 0.214\,\mathrm{eV}\ . \tag{141}$$

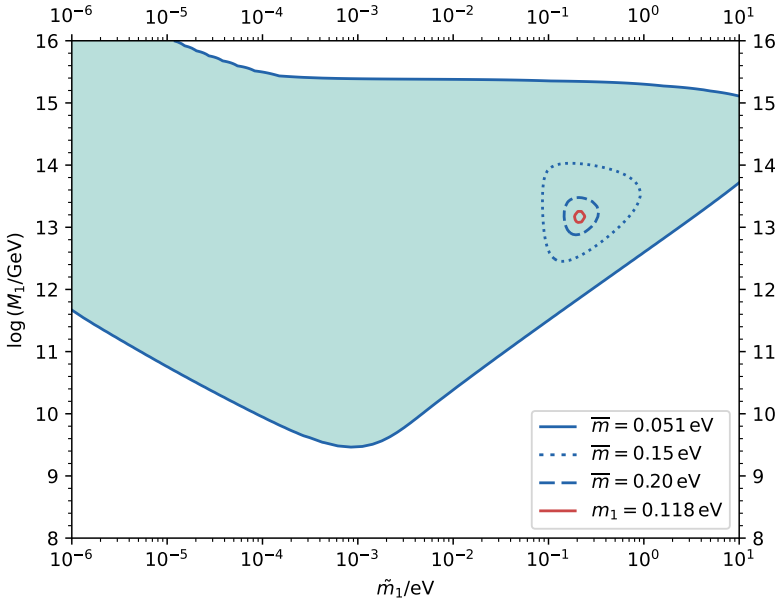

(a)

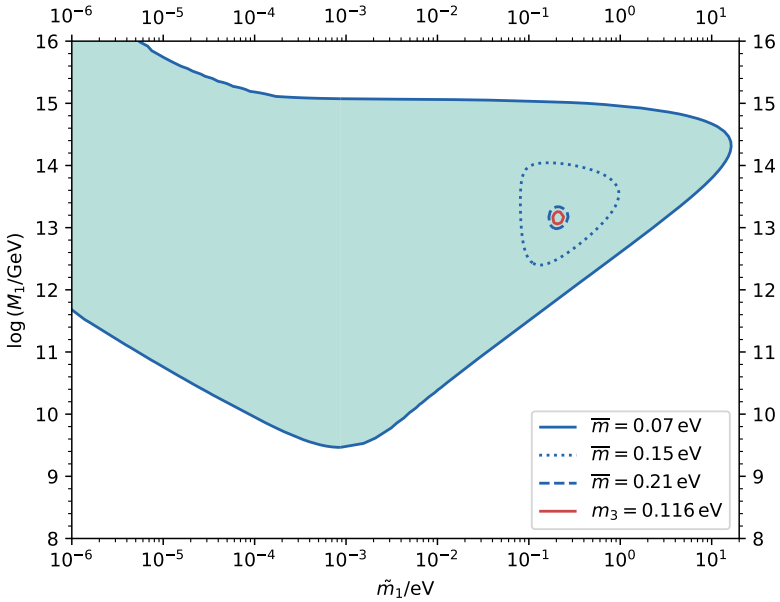

(b)

Figure 5: $(M_1,\tilde{m}_1)$-plane for different values of the lightest light neutrino mass m. The coloured areas inside the contours mark the allowed regions according to CMB data at 3σ $\eta_B^{\mathrm{CMB},3\sigma} = 6 \cdot 10^{-10}$. Fig. 5a describes NO with no allowed region for $m = 0.119\,\mathrm{eV}$, while fig. 5b describes IO with no allowed region for $m = 0.117\,\mathrm{eV}$. The plots are designed similarly to those of [6] to allow to compare them and evaluate the usage of `ULYSSES`.

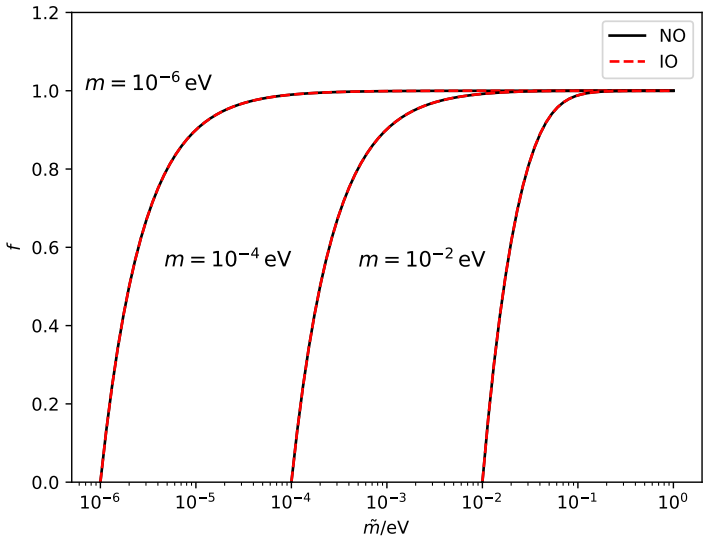

Figure 6: The evolution of $f(\tilde{m}_1, m)$ with $\tilde{m}_1$ is shown for different values of m for NO and IO.

Comparing the results of IO to those of NO, one finds that the bound on $\overline{m}$ is slightly relaxed while for the lightest mass m the bound is slightly tightened.

The shape of the allowed region is determined by $\tilde{m}_1$, M_1 and m via $\varepsilon^{\max}(\tilde{m}_1, M_1, m)$ and $\kappa_f(\tilde{m}_1, M_1\overline{m}^2)$, where $\overline{m}$ is in turn expressed through m. The dependence of $\varepsilon^{\max}(M_1, \tilde{m}_1, m)$ on $\tilde{m}_1$ is located in $f(\tilde{m}_1, m)$, for which $f(\tilde{m}_1, m) \simeq 0$ applies for $\tilde{m}_1 \approx m$ and $f(\tilde{m}_1, m) \simeq 1$ for $\tilde{m}_1 \gg m$. The dependence of f on $\tilde{m}_1$ is shown in fig. 6 both for NO and IO for different masses m. There is no significant difference between NO and IO in the function f if NO and IO are evaluated for the same m. Since $\tilde{m}_1 \geq m$, the allowed region shifts towards higher values of $\tilde{m}_1$ when increasing m. Additionally, $\beta_{\max}$ also drops off for increasing m leading to an overall suppression of the entire allowed region. The evolution is depicted in fig. 7. Here it can be observed that $\beta_{\max}$ is always larger for NO than for IO and for $m \to \infty$ the ratio NO/IO reaches the value $m_{\text{atm}}^{\text{NO}}/m_{\text{atm}}^{\text{IO}} \simeq 1.0034$. When comparing NO to IO, this factor also arises because of $\varepsilon'(M_1) \propto m_{\text{atm}}$. Therefore the allowed region is increased for NO and subsequently the upper bound on the light neutrino masses is relaxed.

Another important factor is κ_f. Along the $\tilde{m}_1$-axis of the ($\tilde{m}_1$,M_1)-plane η_B follows the course of κ_f as depicted in fig. 4. This is particularly evident in the case of $m = 0\,\text{eV}$, where $f = 1$, $\beta_{\max} = 1$, $\varepsilon^{\max} = \varepsilon'(M_1)$. Then, η_B grows larger with increasing $\tilde{m}_1$ up to approximately $\tilde{m}_1 \simeq 10^{-3}$. In

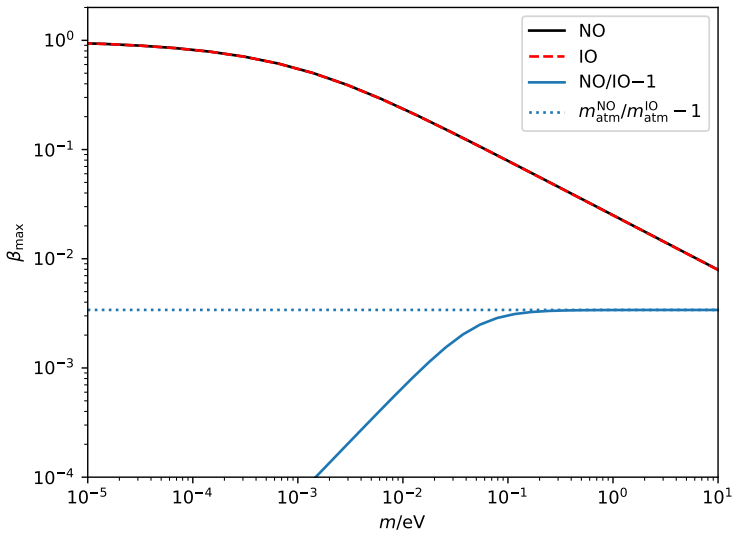

Figure 7: The suppression factor $\beta_{\max}$ of $\varepsilon^{\max}$ is depicted as function of m and compared for NO and IO. For large m the relation reaches $m^{\mathrm{NO}}_{\mathrm{atm}}/m^{\mathrm{IO}}_{\mathrm{atm}}$.

the strong washout regime η_B falls off with increasing $\tilde{m}_1$ because of the washout processes and, eventually, the allowed region vanishes completely. This is only visible for $M_1 \lesssim 10^{14}\,\mathrm{GeV}$ however because of the $\Delta L = 2$ washout as discussed below.

For a fixed value of $\tilde{m}_1$, η_B increases with rising M_1 since $\varepsilon^{\max} \propto M_1$. Eventually the $\Delta L = 2$ washout $\Delta W \propto M_1 \overline{m}^2$ dominates [7] and reduces η_B again, which limits the allowed region on the M_1-axis. For any given factor of m, $\overline{m}^{\mathrm{IO}}$ exceeds $\overline{m}^{\mathrm{NO}}$. The difference is maximal for $m = 0\,\mathrm{eV}$, where $\overline{m}^{\mathrm{IO}}_0 = 0.070\,\mathrm{eV}$ and $\overline{m}^{\mathrm{NO}}_0 = 0.051\,\mathrm{eV}$. For increasing m the two mass scales approach each other. This behaviour is depicted in fig. 8. Thus, it is possible that in the case of IO m is restricted to lower values and yet still the upper bound on $\overline{m}$ is relaxed in comparison to NO. The dependence of $\overline{m}$ on m in the different mass orderings also explains the observation that IO is restricted to lower RHN masses M_1 by the $\Delta L = 2$ washout than NO for the same m. This is analysed for $m = 0\,\mathrm{eV}$, as in this case the difference between NO and IO is solely due to washout effects [6]. Fig. 9 shows that for $\tilde{m}_1 \lesssim 0.1\,\mathrm{eV}$ the upper bound on $\log(M_1)$ in the case of IO is reduced by an approximate value of 0.32 in comparison to NO. This corresponds to a factor of

$$M_1^{\mathrm{IO,max}} \simeq 0.48 \cdot M_1^{\mathrm{NO,max}} \,, \tag{142}$$

which is in agreement with [6]. The constant factor does not apply for larger $\tilde{m}_1$ because of the other washout processes, which are not dependent on the

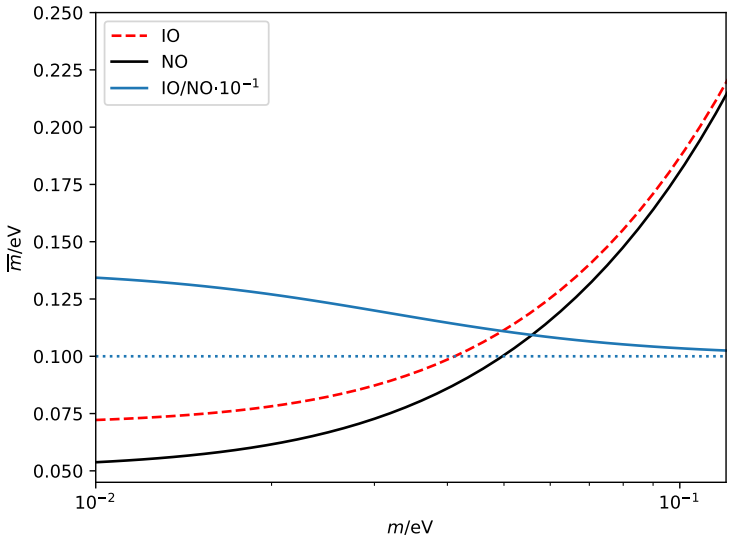

Figure 8: The neutrino mass scale $\overline{m}$ is compared for NO and IO for different values of m.

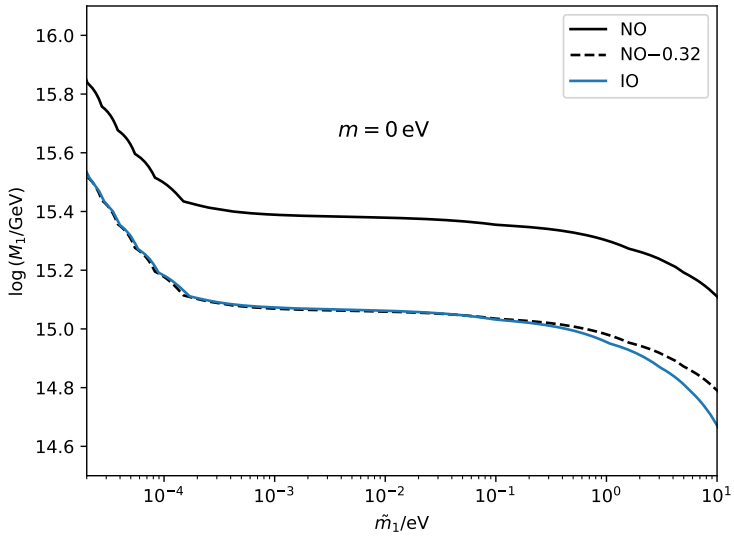

Figure 9: The upper contour lines of NO and IO from 5a and 5b are compared for the largest allowed region with $m = 0\,\mathrm{eV}$.

mass ordering and whose influence affects the contour of IO first due to the lower values of M_1. This also reduces the maximal possible value of $\tilde{m}_1$ for IO [6] in comparison to NO and contributes to the fact that the allowed region vanishes first for IO.

It is possible to determine a lower bound on M_1 by reading off the minimum along the $\tilde{m}_1$-axis for the largest possible allowed region, so for $m = 0\,\text{eV}$. This gives

$$M_1 > 2.88 \cdot 10^9\,\text{GeV}\ , \tag{143}$$

for both NO and IO.

6 Conclusion

This work explores the usefulness of working with `ULYSSES` specifically for finding neutrino mass bounds and reproducing the results of [6]. The main results are the 2 dimensional parameter scans for NO in fig. 5a and for IO in fig. 5b, which very much resemble the corresponding fig. 2 and fig. 4 in [6]. The heavy neutrino mass bound $M_1 > 2.88 \cdot 10^9\,\text{GeV}$ is in good agreement with the results from [7]. The obtained mass bounds for the light neutrinos $m_1, m_2 < 0.119\,\text{eV}$, $m_3 < 0.129\,\text{eV}$ for NO and $m_3 < 0.117\,\text{eV}$, $m_1, m_2 < 0.127\,\text{eV}$ for IO are consistent with the analytical and numerical bounds as presented in [7, 6]. These bounds have been determined up to the third decimal, however it needs to be taken into account that the one-flavour approximation was used and spectator processes, e.g. the sphaleron processes during leptogenesis, have been neglected. The inclusion is estimated to reduce the baryon asymmetry by a factor of 2 [49]. Furthermore, terms like the washout rates ΔW or W_0 were approximated for the strong washout regime. Deviations in the weak washout regime are of less interest however since the bounds are located in the strong washout regime anyways. Thus, the `ULYSSES` code gives reliable results.

It is very simple and straightforward to modify the code to the desired scenario because of its special structuring. On the one side there is the base class `uls-base` together with the different models like `uls-scan2D` which set the technical framework and the definitions of general functions and constants and also deal with the numerical calculation and the output. On the other side, the individual plugins describe the specific physical situation by setting the Boltzmann equations and the initial conditions. Adjustments to the code are then only necessary to the plugins. Additionally, there already exists a great number of plugins for different versions of leptogenesis, which make for a good starting point and simplify creating your own plugin.

Another benefit is the relatively short computation time. On average `ULYSSES` completes approximately 7.2 iterations per second with the adjusted plugin, in each of which it solves the Boltzmann equation for a set of

parameters and takes the final value of the evolution. E.g., each scan for a fixed m in fig. 5a and fig. 5b took about 23 min to complete.

However, the strict set of input parameters proves to be an inconvenience specifically for this analysis, where ε and κ_f are dependent on $\tilde{m}_1$, because $\tilde{m}_1$ can not be accessed directly. This causes a distortion in the distance of the individual data points in the (M_1,$\tilde{m}_1$) plane since one has to work with y_2 or y_3 instead and a convoluted rearrangement of the parameter space is necessary. It would be more convenient to work with $\tilde{m}_1$ as an input parameter directly, which would require a slight rework of `uls-base`.

Overall however, the easy application and the flexibility in the possible physical scenarios presented through different plugins makes `ULYSSES` a useful tool in the analysis of leptogenesis scenarios.

7 Appendix

7.1 A - Set of chemical potentials

Considering all interactions that are in thermal equilibrium in a set temperature region during the evolution of the early universe gives a series of constraints on the chemical potentials of the participating particles [18]. These constraints are expressed with (11), (12), (13) and (16). They can be solved for one arbitrary chemical potential, in this case μ_l. The sums in the equations just give a factor of N_f since the chemical potentials of the quarks are identical for all generations and for the leptons they are assumed to be equal es well [1]. (11) then immediately gives

$$N_f(3\mu_q + \mu_l) = 0 \qquad \Leftrightarrow \qquad \frac{\mu_q}{\mu_l} = -\frac{1}{3} \; . \tag{144}$$

From this and (12) follows

$$N_f(2\mu_q - \mu_u - \mu_d) = 0 \qquad \Leftrightarrow \qquad \frac{\mu_u}{\mu_l} + \frac{\mu_d}{\mu_l} = 2\frac{\mu_q}{\mu_l} = -\frac{2}{3} \; . \tag{145}$$

Next, consider the equation for vanishing hypercharge (16)

$$\begin{aligned} 2\mu_\phi &= N_f(\mu_q + 2\mu_u - \mu_d - \mu_l - \mu_e) \\ &= N_f(2\mu_q - 2(\mu_q - \mu_u) - (-\mu_q + \mu_d) - 2\mu_l - (-\mu_l + \mu_e)) \; . \end{aligned}$$

The relations from the Yukawa interactions (13) are inserted

$$2\mu_\phi = 2N_f(\mu_q - \mu_l - 2\mu_\phi) \; . \tag{146}$$

Using (144) this can be solved for μ_ϕ/μ_l

$$\frac{\mu_\phi}{\mu_l} = -\frac{4N_f}{6N_f + 3} \; . \tag{147}$$

The relations μ_e/μ_l and μ_d/μ_l can be calculated using the above result, (144) and once again the constraint acquired from the Yukawa interaction

$$\frac{\mu_e}{\mu_l} = \frac{\mu_\phi}{\mu_l} + 1 = \frac{2N_f + 3}{6N_f + 3} \; , \tag{148}$$

$$\frac{\mu_d}{\mu_l} = \frac{\mu_\phi}{\mu_l} + \frac{\mu_q}{\mu_l} = -\frac{6N_f + 1}{6N_f + 3} \; . \tag{149}$$

Finally the expression for μ_u/μ_l is found using (145) and (149)

$$\frac{\mu_u}{\mu_l} = -\frac{2}{3} - \frac{\mu_d}{\mu_l} = \frac{2N_f - 1}{6N_f + 3} \; . \tag{150}$$

In order to express the number density of baryons and leptons with just μ_l, the terms (17) and (18) are used which yields

$$n_B = \frac{T^2}{6} N_f \left(2\frac{\mu_q}{\mu_l} + \frac{\mu_u}{\mu_l} + \frac{\mu_d}{\mu_l} \right) \mu_l = -\frac{T^2}{6} \frac{4N_f}{3} \mu_l \ , \tag{151}$$

$$n_L = \frac{T^2}{6} N_f \left(2 + \frac{\mu_e}{\mu_l} \right) \mu_l = \frac{T^2}{6} \frac{14N_f^2 + 9N_f}{6N_f + 3} \mu_l \ . \tag{152}$$

Subtracting (152) from (151) gives

$$n_B - n_L = \frac{T^2}{6} \mu_l \left(-\frac{4N_f}{3} - \frac{14N_f^2 + 9N_f}{6N_f + 3} \right) = -\frac{T^2}{6} \mu_l \frac{22N_f^2 + 13N_f}{6N_f + 3} \ . \tag{153}$$

Finally, with (151), (152) and (153) μ_l can be eliminated from the equations by calculating the ratios of the number densities which also give the ratios of B, L and $B - L$

$$\frac{B}{B-L} = \frac{n_B}{n_B - n_L} = \frac{4N_f}{3} \frac{6N_f + 3}{22N_f^2 + 13N_f} = \frac{8N_f + 4}{22N_f + 13} \equiv c_S \ , \tag{154}$$

$$\frac{L}{B-L} = \frac{n_L}{n_B - n_L} = -\frac{14N_f^2 + 9N_f}{6N_f + 3} \frac{6N_f + 3}{22N_f^2 + 13N_f} = c_S - 1 \ . \tag{155}$$

7.2 B - Deriving ε_i from Feynman diagrams

The CP asymmetry ε_i is defined as in (56) with

$$\varepsilon_i = \frac{\Gamma(N_i \to l\phi) - \Gamma(N_i \to \bar{l}\phi^\dagger)}{\Gamma(N_i \to l\phi) + \Gamma(N_i \to \bar{l}\phi^\dagger)} \ .$$

To calculate the rates $\Gamma(N_i \to l\phi)$ for the decay and its CP inversed $\Gamma(N_i \to \bar{l}\phi^\dagger)$, with the heavy Neutrino N_i, lepton l and the Higgs ϕ, the corresponding Feynman diagrams have to be evaluated, starting with the tree-level diagram from fig. 10. The Feynman rules for Majorana particles are taken from [50].

The interaction between the three particles is described with the Lagrangian [31]

$$\mathcal{L} = -Y_{ji} \epsilon_{\alpha\beta} \overline{N}_i P_L l_j^\alpha \phi^\beta + h.c. \ , \tag{156}$$

where Y_{ji} is the Yukawa coupling, α and β denote the different particles from the respective doublet and j marks the lepton flavours, all of which will be summed over at the end since flavour effects are neglected in the one flavour approximation. $\epsilon_{\alpha\beta}$ ensures the correct selection from the doublets with $\epsilon_{\alpha\beta} = -\epsilon_{\beta\alpha}$ and $\epsilon_{12} = +1$. Because the heavy neutrino mass is larger than 10^9 GeV the calculations are conducted in the symmetric phase where

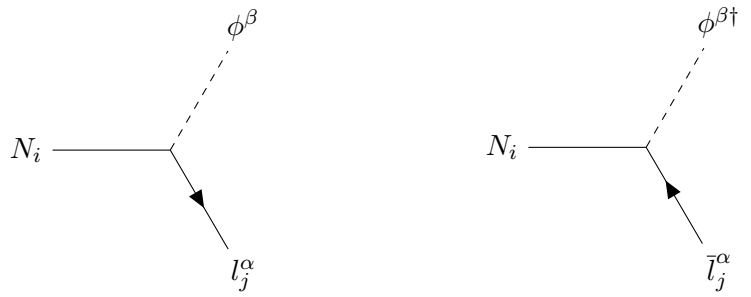

(a) (b)

Figure 10: The tree-level diagram. Fig. 10a shows $\Gamma(N_i \to l\phi)$, fig. 10b shows $\Gamma(N_i \to \bar{l}\phi^\dagger)$ [1].

the mass of the leptons $m_l \simeq 0\,\text{eV}$ and of the Higgs $m_\phi \simeq 0\,\text{eV}$ [31]. For the tree-level diagram the matrix element reads

$$D_1(N_i \to l\phi) = -i\left[\overline{u}_{\alpha,j}(p_1, s_1)(-i)Y^*_{ji}\epsilon_{\alpha\beta}P_R u_i(p, s)\right] \ , \tag{157}$$

where p, s, p_1, s_1 and p_2, s_2 are the momentum and spin of the external RHN, the lepton and the Higgs respectively. This leads to

$$|D_1(N_i \to l\phi)|^2 = (\epsilon_{\alpha\beta})^2(Y^\dagger)_{ij}Y_{ji}\,\text{Tr}[P_R u_i \overline{u}_i P_L u_j^\alpha \overline{u}_j^\alpha] \ . \tag{158}$$

Using Casimir's trick [51] the trace is evaluated and gives

$$\text{Tr}[P_L u_i \overline{u}_i P_R u_j^\alpha \overline{u}_j^\alpha] = 2pp_1 \ . \tag{159}$$

Summing over j and α, β with $\sum_{\alpha,\beta}(\epsilon_{\alpha\beta})^2 = 2$ and including the factor of $1/2$ from the spin average, the averaged squared matrix element reads

$$\langle|D_1(N_i \to l\phi)|^2\rangle = (Y^\dagger Y)_{ii}2pp_1 \ . \tag{160}$$

The reaction rate $\Gamma(N_i \to l\phi)$ is then calculated using Fermi's golden rule [51] to integrate over the momenta p_1 and p_2. In the CMS reference frame this yields

$$\begin{aligned}
\Gamma(N_i \to l\phi) &= \frac{1}{2M_i}\int\langle|D_1(N_i \to l\phi)|^2\rangle(2\pi)^4\frac{\delta^4(p - p_1 - p_2)}{4|\vec{p}_1||\vec{p}_2|}\frac{d\vec{p}_1}{(2\pi)^3}\frac{d\vec{p}_2}{(2\pi)^3} \\
&= \frac{(Y^\dagger Y)_{ii}}{16\pi^2 M_i}\int\frac{pp_1}{|\vec{p}_1||\vec{p} - \vec{p}_1|}\delta(E - E_1 - E_2)d\vec{p}_1 \\
&= \frac{(Y^\dagger Y)_{ii}}{16\pi^2 M_i}\pi M_i^2 \\
&= \frac{(Y^\dagger Y)_{ii}}{16\pi}M_i
\end{aligned} \tag{161}$$

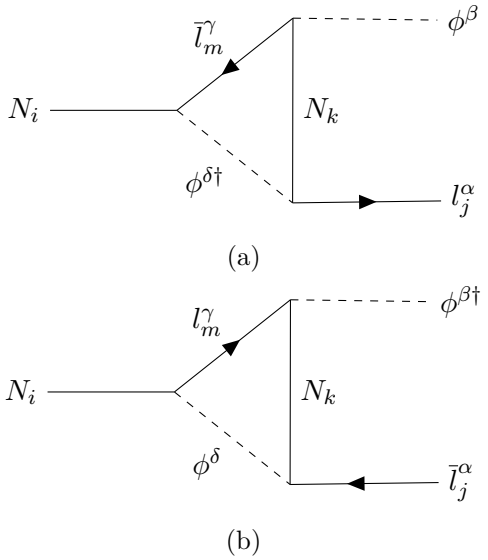

Figure 11: The diagram for the vertex correction with $\Gamma(N_i \to l\phi)$ in fig. 11a and $\Gamma(N_i \to \bar{l}\phi^\dagger)$ in fig. 11b [31].

For the CP inversed reaction rate $\Gamma(N_i \to \bar{l}\phi^\dagger)$ only the expression for the trace is different with

$$\mathrm{Tr}[P_L v_j^\alpha \overline{v}_j^\alpha P_R v_i \overline{v}_i] \ . \tag{162}$$

After applying Casimir's trick however, one receives the same result $2pp_1$. Therefore

$$\Gamma(N_i \to \bar{l}\phi^\dagger) = \Gamma(N_i \to l\phi) = \frac{(Y^\dagger Y)_{ii}}{16\pi} M_i \tag{163}$$

and hence

$$\varepsilon_i(tree) = 0 \ . \tag{164}$$

To extend the calculation up to leading order, the interference terms of the vertex correction and the wave function piece must be considered. The matrix elements of the corrections are D_2 for the vertex and D_3 for the wave function. The matrix element including the interference terms as expansion then reads

$$|\mathcal{M}|^2 = |D_1|^2 + 2\,\mathrm{Re}[D_2 D_1^\dagger] + 2\,\mathrm{Re}[D_3 D_1^\dagger] \ . \tag{165}$$

The Feynman diagrams for the vertex correction are depicted in fig. 11. The internal momentum q of the Higgs propagator leads to an integral in the averaged matrix element. It is useful to consider the correction to the asymmetry $\varepsilon_i(vertex)$ first before evaluating the integrals, as some contributions from $\Gamma(N_i \to l\phi)$ and $\Gamma(N_i \to \bar{l}\phi^\dagger)$ will cancel each other out. After evaluating the sum over α and β but keeping the internal integrals I as such

the spin averages read

$$\langle D_2 D_1^\dagger(N_i \to l\phi)\rangle = i\frac{1}{(2\pi)^4}(Y^\dagger Y)^2_{ki} I^{l\phi} \ , \tag{166}$$

$$\langle D_2 D_1^\dagger(N_i \to \bar{l}\phi^\dagger)\rangle = i\frac{1}{(2\pi)^4}(Y^\dagger Y)^2_{ik} I^{\bar{l}\phi^\dagger} \ , \tag{167}$$

where the factor $1/(2\pi)^4$ is pulled out of the internal integral over q. To go to the full rates Γ Fermi's golden rule is applied and integrating over the external momenta p_1 and p_2 together with the prefactors gives a factor of $1/(16\pi M_i)$. Also, the conservation laws set $p^2 = M_i^2$, $pp_1 = M_i^2/2$ and $p_1^2 \simeq 0$ in the CMS reference frame. Additionally, the difference of the rates is divided by their sum, which is taken from the tree-level diagrams. This gives another factor of $8\pi/(M_i(Y^\dagger Y)_{ii})$. The asymmetry then reads

$$\begin{aligned}
\varepsilon_i &= \frac{1}{(2\pi)^4}\sum_k \frac{1}{M_i^2 (Y^\dagger Y)_{ii}} \{\mathrm{Re}(i(Y^\dagger Y)^2_{ki} I^{l\phi}) - \mathrm{Re}(i(Y^\dagger Y)^2_{ik} I^{\bar{l}\phi^\dagger})\} \\
&= \frac{1}{(2\pi)^4}\sum_k \frac{1}{M_i^2 (Y^\dagger Y)_{ii}} \cdot \\
&\cdot \{[-\mathrm{Im}(I^{l\phi}) + \mathrm{Im}(I^{\bar{l}\phi^\dagger})]\,\mathrm{Re}((Y^\dagger Y)^2_{ki}) - [\mathrm{Re}(I^{l\phi}) + \mathrm{Re}(I^{\bar{l}\phi^\dagger})]\,\mathrm{Im}((Y^\dagger Y)^2_{ki})\}
\end{aligned} \tag{168}$$

The first integral $I^{l\phi}$ is

$$\begin{aligned}
I^{l\phi} =& \int d^4q \{16[(p_1-q)^2 - M_k^2](p-q)^2 q^2\}^{-1} \cdot \\
&\cdot \mathrm{Tr}[(1+\gamma^5)(\not{p}_1 - \not{q} + M_k)(1+\gamma^5)(\not{p} - \not{q})(1-\gamma^5)(\not{p} + M_i)(1-\gamma^5)\not{p}_1)] \\
=& 2M_k M_i \int d^4q \frac{p_1(p-q)}{[(p_1-q)^2 - M_k^2](p-q)^2 q^2} \ .
\end{aligned} \tag{169}$$

The second integral $I^{\bar{l}\phi^\dagger}$ only differs in the formulation of the trace, the solution however is the same with

$$\begin{aligned}
I^{\bar{l}\phi^\dagger} =& \int d^4q \{16[(p_1-q)^2 - M_k^2](p-q)^2 q^2\}^{-1} \cdot \\
&\cdot \mathrm{Tr}[(1+\gamma^5)(\not{q} - \not{p})(1-\gamma^5)(-\not{p}_1 + \not{q} + M_k)(1-\gamma^5)\not{p}_1(1+\gamma^5)(\not{p} - M_i)] \\
=& 2M_k M_i \int d^4q \frac{p_1(p-q)}{[(p_1-q)^2 - M_k^2](p-q)^2 q^2} \ ,
\end{aligned} \tag{170}$$

and therefore $I^{l\phi} = I^{\bar{l}\phi^\dagger}$. Thus, in (168) the imaginary part of the integral vanishes. The next step is to use the Feynman parameterisation [52] to

rewrite the above stated integral as

$$4M_kM_i\int_0^1 dy\int_0^{1-y} dx\int d^4q\frac{p_1(p-q)}{[q^2-2qa+b]^3}\ , \tag{171}$$

where

$$a = xp_1 + yp\ , \tag{172}$$

$$b = yM_i^2 - xM_k^2\ . \tag{173}$$

Substituting $q = l + a$ and subsequently performing a Wick rotation [52] gives an integral in euclidean geometry

$$\begin{aligned}&8M_kM_i i\pi^2\int_0^1 dy\int_0^{1-y} dx[p_1p - p_1(xp_1+yp)]\int_0^\infty \frac{l_E^3}{[-l_E^2+b-a^2]^3}d^4l_E\\ =&2M_kM_i i\pi^2\int_0^1 dy\int_0^{1-y} dx\frac{p_1p-p_1(xp_1+yp)}{b-a^2}\ .\end{aligned} \tag{174}$$

The above mentioned relations for p^2, pp_1 and p_1^2 simplify the integration over x and give

$$\begin{aligned}&M_kM_i i\pi^2\int_0^1 dy\int_0^{1-y} dx\frac{y-1}{x(M_k^2/M_i^2+y)+y(y-1)}\\ =&M_kM_i i\pi^2\int_0^1 dy\frac{y-1}{y+M_k^2/M_i^2}\left[\ln\frac{M_k^2}{M_i^2}-\ln y+i\pi\right]\ .\end{aligned} \tag{175}$$

Now one can take just the real part, since the imaginary parts cancel each other out in (168). The complete solution reads

$$\mathrm{Re}(I^{l\phi}) = -M_kM_i\pi^3\left[1-\left(1+\frac{M_k^2}{M_i^2}\right)\ln\left(\frac{1+M_k^2/M_i^2}{M_k^2/M_i^2}\right)\right]\ , \tag{176}$$

and the result for the asymmetry is

$$\varepsilon_i(vertex) = \frac{1}{8\pi}\sum_k\frac{M_k}{M_i}\left[1-\left(1+\frac{M_k^2}{M_i^2}\right)\ln\left(\frac{1+M_k^2/M_i^2}{M_k^2/M_i^2}\right)\right]\frac{\mathrm{Im}[(Y^\dagger Y)_{ki}^2]}{(Y^\dagger Y)_{ii}}\ . \tag{177}$$

For the wave function correction the procedure is the same. The diagrams are depicted in fig. 12.

Once again it is necessary to integrate over the internal momentum q of the Higgs. Inside the loop both combinations of l_m^γ, ϕ^δ and $\bar{l}_m^\gamma$, $\phi^{\beta\dagger}$ are possible. The corresponding internal integrals are denoted with the subscripts 1,2 for l,ϕ and $\bar{l}$, $\phi^\dagger$ respectively. For the matrix element both cases have to be evaluated and summed over. The spin average of the interference terms yield

$$\langle D_3D_1^\dagger(N_i\to l\phi)\rangle = i\frac{2}{(2\pi)^4}[(Y^\dagger Y)_{ik}(Y_{jk}^*Y_{ji})I_1^{l\phi} + (Y^\dagger Y)_{ki}(Y_{jk}^*Y_{ji})I_2^{l\phi}] \tag{178}$$

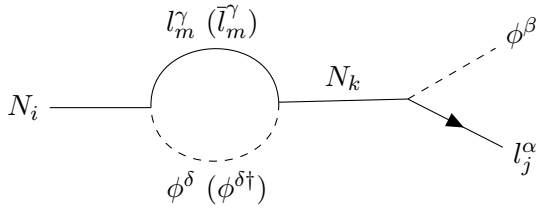

(a)

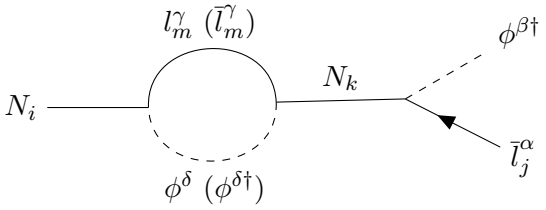

(b)

Figure 12: The diagram for the wave function correction. Fig. 12a depicts $\Gamma(N_i \to l\phi)$, 12b depicts $\Gamma(N_i \to \bar{l}\phi^\dagger)$. The loop can contain both l,ϕ and $\bar{l}$, $\phi^\dagger$ [31].

and

$$\langle D_3 D_1^\dagger (N_i \to \bar{l}\phi^\dagger)\rangle = i\frac{2}{(2\pi)^4}[(Y^\dagger Y)_{ik}(Y_{jk}^* Y_{ji})^* I_1^{\bar{l}\phi^\dagger} + (Y^\dagger Y)_{ki}(Y_{jk}^* Y_{ji})^* I_2^{\bar{l}\phi^\dagger}] \tag{179}$$

To go to Γ the real part is taken and both terms receive the prefactors $1/(16\pi M_i)$ and $8\pi/(M_i(Y^\dagger Y)_{ii})$ from the integral over external momenta and from dividing by the sum of the tree-level rates. Then, summing over $k \neq i$ as well as α, β, γ and δ, the asymmetry reads

$$\begin{aligned}\varepsilon_i = \frac{2}{(2\pi)^4}\sum_{k\neq i}\frac{1}{M_i^2 (Y^\dagger Y)_{ii}}\cdot \\ \cdot[\mathrm{Re}(i(Y^\dagger Y)_{ik}(Y_{jk}^* Y_{ji}) I_1^{l\phi}) + \mathrm{Re}(i(Y^\dagger Y)_{ki}(Y_{jk}^* Y_{ji}) I_2^{l\phi}) \\ - \mathrm{Re}(i(Y^\dagger Y)_{ik}(Y_{jk}^* Y_{ji})^* I_1^{\bar{l}\phi^\dagger}) - \mathrm{Re}(i(Y^\dagger Y)_{ki}(Y_{jk}^* Y_{ji})^* I_2^{\bar{l}\phi^\dagger})]\end{aligned}$$

The real parts are brought into a more convenient form

$$\begin{aligned}\mathrm{Re}(i(Y^\dagger Y)_{ik}(Y_{jk}^* Y_{ji}) I_1^{l\phi}) = &- \mathrm{Re}(I_1^{l\phi})\,\mathrm{Im}((Y^\dagger Y)_{ik}(Y_{jk}^* Y_{ji})) \\ &- \mathrm{Im}(I_1^{l\phi})\,\mathrm{Re}((Y^\dagger Y)_{ik}(Y_{jk}^* Y_{ji}))\ ,\end{aligned} \tag{180}$$

$$\begin{aligned}\mathrm{Re}(i(Y^\dagger Y)_{ki}(Y_{jk}^* Y_{ji}) I_2^{l\phi}) = &- \mathrm{Re}(I_2^{l\phi})\,\mathrm{Im}((Y^\dagger Y)_{ki}(Y_{jk}^* Y_{ji})) \\ &- \mathrm{Im}(I_2^{l\phi})\,\mathrm{Re}((Y^\dagger Y)_{ki}(Y_{jk}^* Y_{ji}))\ ,\end{aligned} \tag{181}$$

$$\begin{aligned}\mathrm{Re}(i(Y^\dagger Y)_{ik}(Y^*_{jk}Y_{ji})^* I_1^{\bar{l}\phi^\dagger}) = &+ \mathrm{Re}(I_1^{\bar{l}\phi^\dagger})\,\mathrm{Im}((Y^\dagger Y)_{ki}(Y^*_{jk}Y_{ji})) \\ &- \mathrm{Im}(I_1^{\bar{l}\phi^\dagger})\,\mathrm{Re}((Y^\dagger Y)_{ki}(Y^*_{jk}Y_{ji}))\ ,\end{aligned} \tag{182}$$

$$\begin{aligned}\mathrm{Re}(i(Y^\dagger Y)_{ki}(Y^*_{mk}Y_{mi})^* I_2^{\bar{l}\phi^\dagger}) = &+ \mathrm{Re}(I_2^{\bar{l}\phi^\dagger})\,\mathrm{Im}((Y^\dagger Y)_{ik}(Y^*_{jk}Y_{ji})) \\ &- \mathrm{Im}(I_2^{\bar{l}\phi^\dagger})\,\mathrm{Re}((Y^\dagger Y)_{ik}(Y^*_{jk}Y_{ji}))\ .\end{aligned} \tag{183}$$

The asymmetry is expressed with

$$\begin{aligned}\varepsilon_i = \frac{2}{(2\pi)^4}\sum_{k\neq i}\frac{1}{M_i^2(Y^\dagger Y)_{ii}}\cdot\{&-[\mathrm{Re}(I_1^{l\phi}) + \mathrm{Re}(I_2^{\bar{l}\phi^\dagger})]\,\mathrm{Im}((Y^\dagger Y)_{ik}(Y^*_{jk}Y_{ji})) \\ &- [\mathrm{Im}(I_1^{l\phi}) - \mathrm{Im}(I_2^{\bar{l}\phi^\dagger})]\,\mathrm{Re}((Y^\dagger Y)_{ik}(Y^*_{jk}Y_{ji})) \\ &- [\mathrm{Re}(I_2^{l\phi}) + \mathrm{Re}(I_1^{\bar{l}\phi^\dagger})]\,\mathrm{Im}((Y^\dagger Y)_{ki}(Y^*_{jk}Y_{ji})) \\ &- [\mathrm{Im}(I_2^{l\phi}) - \mathrm{Im}(I_1^{\bar{l}\phi^\dagger})]\,\mathrm{Re}((Y^\dagger Y)_{ki}(Y^*_{jk}Y_{ji}))\}\ .\end{aligned} \tag{184}$$

Now, the integrals have to be solved specifically. The integral $I_1^{l\phi}$ reads

$$I_1^{l\phi} = \int d^4q \frac{\mathrm{Tr}[(1+\gamma^5)(\not{p}_1 + M_k)(1-\gamma^5)(\not{p}-\not{q})(1+\gamma^5)(\not{p}+M_i)(1-\gamma^5)\not{p}_1]}{16(p^2-M_k^2)(p-q)^2q^2}\ . \tag{185}$$

The other integrals only differ in the terms for the trace. The evaluated traces are listed below in the order $I_1^{l\phi}$, $I_2^{l\phi}$, $I_1^{\bar{l}\phi^\dagger}$ and $I_2^{\bar{l}\phi^\dagger}$:

$$\begin{aligned}&\mathrm{Tr}[(1+\gamma^5)(\not{p}+M_k)(1-\gamma^5)(\not{p}-\not{q})(1+\gamma^5)(\not{p}+M_i)(1-\gamma^5)\not{p}_1] \\ &\quad = 32[p^2(pp_1+qp_1) - 2(pq)(pp_1)]\ ,\end{aligned} \tag{186}$$

$$\begin{aligned}&\mathrm{Tr}[(1+\gamma^5)(\not{p}+M_k)(1+\gamma^5)(\not{p}-\not{q})(1-\gamma^5)(\not{p}+M_i)(1-\gamma^5)\not{p}_1] \\ &\quad = 32M_iM_kp_1(p-q)\ ,\end{aligned} \tag{187}$$

$$\begin{aligned}&\mathrm{Tr}[(1+\gamma^5)(\not{q}-\not{p})(1-\gamma^5)(-\not{p}+M_k)(1-\gamma^5)\not{p}_1(1+\gamma^5)(\not{p}-M_i)] \\ &\quad = 32M_iM_kp_1(p-q)\ ,\end{aligned} \tag{188}$$

$$\begin{aligned}&\mathrm{Tr}[(1-\gamma^5)(\not{q}-\not{p})(1+\gamma^5)(-\not{p}+M_k)(1-\gamma^5)\not{p}_1(1+\gamma^5)(\not{p}-M_i)] \\ &\quad = 32[p^2(pp_1+qp_1) - 2(pq)(pp_1)]\ .\end{aligned} \tag{189}$$

Then, substituting $q = l + a$ with $a = p(1-x)$, using the Feynman parameterisation and performing a Wick rotation, the integrals become

$$I_1^{l\phi} = I_2^{\bar{l}\phi^\dagger} = \frac{M_i^4}{M_i^2 - M_k^2}\chi\ , \tag{190}$$

$$I_2^{l\phi} = I_1^{\bar{l}\phi^\dagger} = \frac{M_i^3 M_k}{M_i^2 - M_k^2}\chi \ , \tag{191}$$

with

$$\chi = i\int_0^1 dx \int d^4 l_E \frac{1}{(l_E^2+\Lambda)^2} \quad , \quad \Lambda = M_i^2 x(x-1) \ . \tag{192}$$

This is solved with dimensional regularisation [52], changing the dimensions to $d = 4-\epsilon$. A new factor μ^ϵ is introduced and χ is calculated using the surface element of a d dimensional sphere $d\Omega_{d-1}$

$$\begin{aligned}
\chi =& i\int_0^1 x dx \mu^\epsilon \int d\Omega_{d-1} \int_0^\infty \frac{l_E^{d-1}}{(l_E^2-\Lambda)^2} d^d l_E \\
=& i\int_0^1 x dx \frac{2\pi^{d/2}}{\Gamma(d/2)} (-\Lambda)^{d/2-2} \frac{\mu^\epsilon}{2} \Gamma(2-d/2)\Gamma(d/2) \\
=& i\pi^2 \int_0^1 x dx \left(\frac{\mu^2}{-\Lambda\pi}\right)^\epsilon 2\Gamma(\epsilon/2) \ .
\end{aligned} \tag{193}$$

The expression is expanded up to $\mathcal{O}(\epsilon^0)$. Then, the final integration over x can be conducted with the result

$$\begin{aligned}
\chi &= i\pi^2 \int_0^1 x \left(\Delta_\varepsilon + \ln\left(\frac{\mu^2}{M_i^2 x(x-1)4\pi^2}\right)\right) dx \\
&= \frac{i\pi^2}{2}(\Delta_\varepsilon + \ln(\mu^2/M_i^2) - \ln(4\pi^2) + 2) - \frac{\pi^3}{2} \ .
\end{aligned} \tag{194}$$

The term Δ_ϵ localises the diverging terms from the expansion

$$\Delta_\epsilon = \frac{2}{\epsilon} - \gamma_E + \ln(4\pi) \ , \tag{195}$$

with γ_E from the expansion of the Γ-function. From (184), (190) and (191) one can see that the imaginary part of χ is cancelled out and only the real part remains. Then, the final result is

$$\varepsilon_i(wave) = -\frac{1}{8\pi}\sum_{k\neq i} \frac{M_i}{M_k^2 - M_i^2} \frac{\mathrm{Im}\{[M_k (Y^\dagger Y)_{ki} + M_i (Y^\dagger Y)_{ik}] Y_{jk}^* Y_{ji}\}}{(Y^\dagger Y)_{ii}} \ . \tag{196}$$

7.3 C - Reformulation of the kinetic equations

In section 4.2 the Boltzmann equations for leptogenesis have been derived as

$$\dot{n}_N + 3Hn_N = -\left(\frac{n_N}{n_N^{eq}} - 1\right)(\gamma_N + \gamma_{\Delta L=1})$$

and

$$\dot{n}_{B-L} + 3Hn_{B-L} = -\varepsilon \left(\frac{n_N}{n_N^{eq}} - 1 \right) \gamma_N \\ - \frac{n_{B-L}}{n_l^{eq}} \left(\frac{1}{2}\gamma_N + 2\gamma_{\Delta L=1,t} + \frac{n_N}{n_N^{eq}}\gamma_{\Delta L=1,s} + \gamma_{\Delta L=2} \right) \ .$$

The goal of this section is to present the steps necessary to simplify the equations to the final result (86) and (87). Instead of investigating the reaction densities and number densities, it is easier to take a look at the number N_N and N_{B-L} in a comoving volume space occupied by one photon. This way, the dynamics of the expansion of the universe presented by the Hubble parameter H can be separated from the equation. The expression for the number N_x is [1]

$$N_x = 2\frac{n_x}{n_\gamma} \ . \tag{197}$$

The relations between the reaction densities γ and the reaction rates per time and particle Γ are [1, 34]

$$\begin{aligned} \Gamma_N = \frac{\gamma_N}{n_N^{eq}} \quad , \quad \Gamma_S = \frac{2\gamma_{\Delta L=1,s} + 4\gamma_{\Delta L=1,t}}{n_N^{eq}} \ , \\ \Gamma_W = \frac{1}{n_l^{eq}} \left(\frac{1}{2}\gamma_N + 2\gamma_{\Delta L=1,t} + \frac{n_N}{n_N^{eq}}\gamma_{\Delta L=1,s} + \gamma_{\Delta L=2} \right) \ . \end{aligned} \tag{198}$$

This immediately results in

$$\frac{d}{dt}(n_\gamma N_N) + 3Hn_\gamma N_N = -(\Gamma_N + \Gamma_S)(n_\gamma N_N - n_\gamma N_N^{eq}) \ , \tag{199}$$

$$\frac{d}{dt}(n_\gamma N_{B-L}) + 3Hn_\gamma N_{B-L} = -\varepsilon\Gamma_N(n_\gamma N_N - n_\gamma N_N^{eq}) - n_\gamma N_{B-L}\Gamma_W \ . \tag{200}$$

Using the product rule the derivatives dn_γ/dt arise. The number density of photons as relativistic particles in the radiation dominated era reads [8]

$$n_\gamma = g\frac{\zeta(3)T^3}{\pi^2} \ , \tag{201}$$

with the degrees of freedom g. The scale factor in this era is $a \propto T^{-1}$ [8] and therefore

$$n_\gamma a^3 = const \ . \tag{202}$$

This represents that the number of photons in the comoving volume space remains constant. Now the derivative is evaluated as

$$\frac{dn_\gamma}{dt} = -\frac{n_\gamma}{a^3}\frac{d(a^3)}{dt} = -3Hn_\gamma \ , \tag{203}$$

Furthermore, the evolution of N_N and N_{B-L} is described with respect to the dimensionless parameter $z = M_1/T$. Changing the variables gives an additional factor of

$$\frac{dN_x}{dt} = \frac{dN_x}{dz}\frac{dz}{dt} = \frac{dN_x}{dz} Hz \ . \tag{204}$$

The relation holds since $z/a = M/(aT) = const$ because $a \propto T^{-1}$ and thus

$$\frac{dz}{dt} = -za\frac{d(a^{-1})}{dt} = zH \ . \tag{205}$$

Inserting (203) and (204) into (199) and (200) and subsequently dividing by n_γ yields

$$\frac{dN_N}{dz} Hz = -(\Gamma_D + \Gamma_S)(N_N - N_N^{eq}) \ , \tag{206}$$

$$\frac{dN_{B-L}}{dz} Hz = -\varepsilon\Gamma_N(N_N - N_N^{eq}) - N_{B-L}\Gamma_W \ . \tag{207}$$

Lastly, to remove all H, rescaled reaction rates are defined [1]

$$D = \frac{\Gamma_D}{Hz} \quad , \quad S = \frac{\Gamma_S}{Hz} \quad , \quad W = \frac{\Gamma_W}{Hz} \ , \tag{208}$$

which then leads to the final result

$$\frac{dN_N}{dz} = -(D + S)(N_N - N_N^{eq}) \ , \tag{209}$$

$$\frac{dN_{B-L}}{dz} = -\varepsilon D(N_N - N_N^{eq}) - WN_{B-L} \ . \tag{210}$$

7.4 D - `etaB1BE1F.py` code

The original code from `etaB1BE1F.py` [4] is displayed here. This code is used as a starting point and modified with the adjustments mentioned in section 5.2.

```
# non-resonant leptogenesis with one decaying sterile neutrino
    using the Boltzmann equations and neglecting flavour
    effects.
import ulysses
import numpy as np
from odeintw import odeintw


from ulysses.numba import jit
@jit
def fast_RHS(y0, d, w1, n1eq, epstt,epsmm,epsee):
    N1      = y0[0]
    NBL     = y0[1]

    rhs1 =                          -d*(N1-n1eq)
```

```
    rhs2 =    (epstt+epsmm+epsee)*d*(N1-n1eq)-w1*NBL

    return [rhs1, rhs2]

class EtaB_1BE1F(ulysses.ULSBase):
    """
    Boltzmann equation (BE) with one decaying sterile. See
    arxiv:1112.4528
    Eqns. 4 and 5.  Note these kinetic equations do not include
     off diagonal
    flavour oscillations.
    """

    def shortname(self): return "1BE1F"

    def flavourindices(self): return [1]

    def flavourlabels(self): return ["$NBL$"]

    def RHS(self, y0,z,epstt,epsmm,epsee,k):

        if z != self._currz or z == self.zmin:
            self._d       = np.real(self.D1(k,z))
            self._w1      = np.real(self.W1(k,z))
            self._n1eq    = self.N1Eq(z)
            self._currz=z
        return fast_RHS(y0, self._d, self._w1, self._n1eq,
    epstt,epsmm,epsee)

    @property
    def EtaB(self):
        #Define fixed quantities for BEs
        epstt = np.real(self.epsilon1ab(2,2))
        epsmm = np.real(self.epsilon1ab(1,1))
        epsee = np.real(self.epsilon1ab(0,0))
        print(epstt, (epstt+epsmm+epsee))
        k       = np.real(self.k1)
        y0      = np.array([0+0j,0+0j], dtype=np.complex128)

        params  = np.array([epstt,epsmm,epsee,k], dtype=np.
    complex128)

        ys      = odeintw(self.RHS, y0, self.zs, args = tuple(
    params), atol=1e-14, rtol = 1e-10)
        self.setEvolData(ys)
        return self.ys[-1][-1]
```